https://doi.org/10.5194/egusphere-2026-1877
Preprint. Discussion started: 29 July 2026

A new ocean model configuration for management of central North Pacific Marine Resources (MOM6-COBALT-HIC6kv1.0)

Gabriela Negrete García[1], Dax Matthews[2,3], Charles A. Stock[1], Brian Powell[2], Ryan R. Rykaczewski[3], Kisei Tanaka[3], Hannah Barkley[3], Tobias Friedrich[2], Jessica Y. Luo[1], Andrew C. Ross[1], Yi-Cheng Teng[1]

[1]NOAA/OAR/GFDL, 201 Forrestal Rd, Princeton, NJ 08540
[2]Department of Oceanography, University of Hawai`i at Manoa, 1000 Pope Road, Marine Sciences Building, Honolulu, HI 96822
[3] Pacific Islands Fisheries Science Center, 1845 Wasp Boulevard Building 176, Honolulu HI 96818

Correspondence to: Gabriela Negrete García (Gabriela.Negrete@noaa.gov)

Abstract. Despite often being referred to as an "ocean desert", the North Pacific Subtropical Gyre (NPSG) supports economically valuable fisheries worth hundreds of millions of dollars annually, including Pacific bigeye tuna (*Thunnus obesus*) and other high-value pelagic species. The waters in and around the Hawaiian Islands support valuable and culturally significant nearshore fisheries and coral reef ecosystems and fuel ocean recreation and tourism valued in the billions. To be useful in understanding and managing these interacting resources, models must adequately represent ocean dynamics across multiple scales, from basin-wide circulation patterns to finer-scale island-ocean interactions. We evaluate the capacity of an ocean and biogeochemical model with 6 km horizontal grid spacing, a resolution considered "high" for climate-scale applications, across these scales. After a number of adjustments, including but not limited to calibrating light attenuation to subtropical observations and adjusting wind forcing to better reflect wind-current feedbacks, the model demonstrates strong skill in capturing basin-scale pelagic habitat features, including seasonal sea surface temperature anomalies ($r > 0.95$), accurate Transition Zone Chlorophyll Front migration and anomalies, and oxycline structure critical for bigeye tuna habitat compression. It also captures key features of the high seas ecosystems as represented by observations at station ALOHA, including exceptionally deep chlorophyll maxima (DCM) and seasonal variations and trends in acidification, though modest biases are evident. At the scale of island-ocean interactions, the model captures heightened eddy kinetic energy (EKE) downstream of the Hawaiian Islands and elevated productivity associated with the island mass effect. Finally, in nearshore regions, the model captures 88% of the temperature variance observed at coral bleaching and habitat monitoring stations despite limited resolution. Overall, the configuration provides a robust foundation for a range of marine resource applications. Potential directions for future improvement include incorporating time-varying biogeochemical boundary conditions, refining salinity dynamics and carbonate chemistry representation, along with continued enhancement of nearshore circulation processes.

Keywords: Ocean modeling, Pacific Islands, model validation, mesoscale processes, island effects, nearshore dynamics, biogeochemistry

1. Introduction

The North Pacific Subtropical Gyre (NPSG) is an oceanographically complex and biologically diverse marine environment that covers most of the northern Pacific Ocean and represents the largest ecosystem on Earth. This vast gyre is characterized by a clockwise circulation pattern formed by four major ocean currents: the North Pacific Current to the north, the California Current to the east, the North Equatorial Current to the south, and the Kuroshio

https://doi.org/10.5194/egusphere-2026-1877
Preprint. Discussion started: 29 July 2026

Current to the west. Located in the southeastern portion of the NPSG, the Hawaiian Islands Chain (HIC) plays an important role in shaping regional oceanic and atmospheric circulation. The islands block the flow of the North Equatorial Current and disrupt the persistent northeast trade winds, producing distinctive circulation patterns in both the atmosphere and the ocean (Xie et al., 2001). This region hosts some of the world's most economically valuable fisheries, with annual landings valued at more than a billion dollars, including Pacific bigeye tuna (*Thunnus obesus*; targeted by Hawai'i's deep-set longline fleet), yellowfin tuna (*Thunnus albacares*), mahimahi (*Coryphaena spp.*), ono (*Acanthocybium solandri*), swordfish (*Xiphias gladius*; targeted by Hawai'i's shallow-set longline fleet), and skipjack tuna (*Katsuwonus pelamis*), as well as other pelagic and demersal species that form the backbone of Pacific Island economies and food security (Williams & Terawasi, 2017).

The oceanographic complexity of this region emerges from the intersection of multiple physical and biogeochemical processes operating across vastly different spatial and temporal scales. This range of scales is mirrored in the layers and overlapping structure of fisheries governance in the region. Highly migratory species such as tunas and billfishes fall under the management jurisdiction of international bodies like the Western and Central Pacific Fisheries Commission and the Inter-American Tropical Tuna Commission. The Western Pacific Regional Fishery Management Council partitions US federal management responsibility across finer scales in the region, from open-ocean pelagic longline fisheries based in US ports, to archipelagic bottomfish, crustacean, precious coral fisheries, and nearshore coral reef habitats that are typically managed by the State of Hawaii. Each tier is shaped by distinct oceanographic dynamics. At the basin scale, the NPSG creates large-scale circulation patterns that control temperature gradients, frontal zones, and primary productivity gradients that determine fish habitat quality (Polovina et al., 2001; Bograd et al., 2004). The oligotrophic core of the NPSG is characterized by downwelling currents, persistent stratification, low nutrient concentrations, and relatively low primary productivity. Despite these conditions, mesoscale and submesoscale features such as eddies, fronts, and filaments can generate localized regions of enhanced productivity through nutrient injection and ecological aggregation mechanisms, supporting remarkably productive fisheries (Karl & Lukas, 1996; Letelier et al., 2004). Poleward of the oligotrophic core, downwelling currents gradually weaken and winter mixing strengthens before conditions change abruptly in the productive North Pacific Transition Zone (NPTZ) separating colder, fresher subarctic water from the NPSG. To the south, the NPSG is bounded by the Pacific equatorial upwelling system and the large-scale open-ocean hypoxic zone underlying it. The westward flowing North Equatorial Current feeds the rapid northward flow Kuroshio current bounding the NPSG to the west, with the California Current upwelling system bounding it to the east.

Superimposed on these basin-scale patterns, numerous islands and seamounts create dramatic modifications to local and regional oceanography through what is collectively known as the "island mass effect" (Doty & Oguri, 1956). Islands generate complex flow patterns including localized upwelling, enhanced vertical mixing, and downstream wakes extending hundreds of kilometers (Xie et al., 2001; Calil et al., 2008; Hasegawa et al., 2009), producing biological hotspots (e.g., elevated chlorophyll and prey availability) that support higher fish biomass and catch rates in many reef systems, creating a stark contrast to the surrounding oligotrophic waters (Gove et al., 2016; Friedlander et al., 2018). The Hawaiian Islands are a particularly well-studied example, since their mountainous topography generates wind-stress curl dipoles, eddy formations, internal wave breaking, and a wind wake that drives the Hawaiian Lee Current and modulates regional ocean-atmosphere dynamics (Xie et al., 2001). These physical processes in turn modulate chlorophyll concentrations, nutrient distributions, thermal fronts, and oxygen gradients across the central North Pacific, influencing pelagic fish availability and catchability through frontal aggregation, thermal habitat constraints, and prey distribution (Seki et al., 2001).

For many commercially important species in this region, open ocean conditions directly determine habitat suitability and catch success. Pacific bigeye tuna, which alone represents a multi-billion dollar industry across Pacific Island nations, exhibits strong associations with specific thermal structure, oxygen levels, and prey distribution patterns (Schaefer et al., 2005; Howell et al., 2010). Their vertical habitat is particularly sensitive to the shoaling of the oxygen minimum zone and thermocline toward the equator, which compresses the available habitat and influences

https://doi.org/10.5194/egusphere-2026-1877
Preprint. Discussion started: 29 July 2026

catchability by longline fisheries (Stramma et al., 2010; Prince & Goodyear, 2006). Similarly, other surface-oriented species like skipjack and yellowfin tuna respond to temperature fronts, productivity gradients, and mesoscale features that concentrate their prey (Dueri et al., 2014; Senina et al., 2020).

In nearshore waters, coral reef habitats and artisanal fisheries are sensitive to temperature variability, storm disturbances, and oceanographic conditions that affect larval recruitment and nutrient delivery (Fox et al., 2012; Hanich et al., 2018). Elevated seawater temperatures can drive coral bleaching and, when thermal stress is sustained, lead to mass coral mortality and reduced habitat complexity. These coastal oceanographic conditions also influence the early life stages of some large pelagic species, including mahimahi and billfish, whose larvae utilize productive nearshore surface slick habitats before migrating to open ocean environments (Whitney et al., 2021). Pacific Island food security depends on both coastal reef fisheries and offshore pelagic fisheries (Bell et al., 2009, 2013), establishing the need for ocean models that resolve conditions from nearshore to basin scales.

Effective management of these valuable fisheries resources requires understanding of how ocean dynamics influence fish distribution, abundance, and catchability across multiple temporal scales. Seasonal cycles, interannual variability driven by climate phenomena like El Niño-Southern Oscillation (ENSO) and the Pacific Decadal Oscillation, and longer-term climate change all affect the productivity and structure of NPSG marine ecosystems (Karl et al., 1995, Corno et al., 2007, Doney et al., 2012). To maximize contributions to effective marine resource management and coastal zone planning, ocean models must capture these multi-scale processes and interactions to a useful degree. The computational expense of these models must also be manageable enough to enable sufficient simulations—including ensemble predictions and projections—to allow a probabilistic characterization of the range of potential ocean futures (Drenkard et al., 2021). Since each doubling of horizontal resolution raises computational costs by an order of magnitude, the design of an ocean modeling system for marine resource applications in the central Pacific resources requires careful balancing of goals and resources.

To advance our understanding of these complex multi-scale interactions and their implications for central Pacific marine resources, we present a new high-resolution regional ocean model that we refer to as the Hawaiian Island Chain 6 kilometer model (HIC6k, Fig. 1). This modeling system, which is based on the Modular Ocean Model version 6 (MOM6; Adcroft et al., 2019) coupled with the Carbon, Ocean Biogeochemistry and Lower Trophics version 3 (COBALTv3) ecosystem model (Stock et al., 2020, 2025), is designed to resolve a spectrum of processes influencing Pacific Island marine ecosystems, from basin-scale subtropical gyre dynamics to fine-scale island-ocean interactions across an extended regional domain. Encompassing the Hawaiian Island Chain (HIC), Northwestern Hawaiian Islands, Johnson Atoll, and critical portions of the NPSG, this vast marine domain spans approximately 5.9°N to 38.8°N latitude, with longitudinal extent varying as a function of latitude due to the curvilinear grid structure ranging from roughly 170°E to 221°E (141°W) at its broadest northern extent to a narrower zonal span near the equatorward boundary (Fig. 1). We pursued a significantly larger domain relative to prior Hawaiian Island configurations used for climate applications (e.g., ~15 times larger than Friedrich et al., 2021, 2024) to capture bigeye tuna fishing grounds and the Northwestern (leeward) Hawaiian Islands that includes the Papahānaumokuākea Marine National Monument. The grid was constructed so that horizontal boundaries sit 10 degrees east and south of the Big Island (the southeasternmost island) and 10 degrees north and west of Kure Atoll (Hōlanikū) — the farthest northwestern island. This larger domain increases computational burden, exacerbating the tensions between resolution and ensemble-based uncertainty approaches.

Our objective is to describe the HIC6k model, emphasizing configuration adjustments relative to prior regional MOM6 configurations (e.g., Ross et al., 2023 for Northwest Atlantic; Drenkard et al., 2025 for Northeast Pacific) that proved critical to skillful pacific islands simulations. We assess baseline configuration performance for fisheries and marine resource applications and identify future development targets that would further enhance this utility. We consider dynamics at three scales. First, we evaluate whether our regional MOM6-COBALT system can accurately resolve the basin-scale dynamics and “high seas” conditions that control pelagic fish habitat across the Pacific

https://doi.org/10.5194/egusphere-2026-1877
Preprint. Discussion started: 29 July 2026

Islands region, including temperature gradients, frontal zones, seasonal variability, and plankton productivity patterns within the domain. Second, we evaluate the model's representation of eddy kinetic energy in island wakes, examining the mesoscale features that can influence regional biogeochemical conditions. Third, we examine whether the model provides sufficient spatial resolution for fundamental coastal applications. Specifically, we ask whether the model can capture time varying hydrographic anomalies observed at coastal observing stations characterizing ocean fluctuations in reef and nearshore habitats.

2. Methods

2.1 Model Description

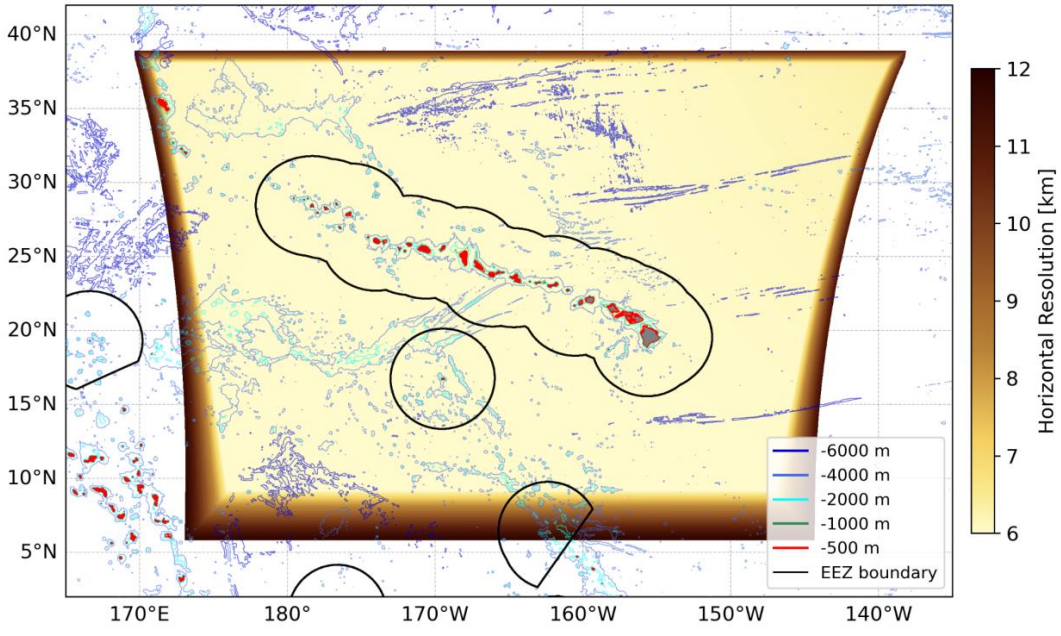

Figure 1. Spatial distribution of model resolution for the MOM6-COBALT 6km configuration in the Pacific Islands Region. The domain uses a curvilinear grid with approximately uniform physical spacing, spanning greater longitudinal extent at higher latitudes than near the equator. Resolution is approximately 6 km throughout the interior (light yellow) and degrades smoothly to ~12 km near the boundaries where sponge layers are applied (dark yellow). Contour lines indicate ocean depth at intervals of −500 m (red), −1000 m (green), −2000 m (cyan), −4000 m (medium blue), and −6000 m (dark blue); black contours delineate U.S. Exclusive Economic Zone (EEZ) boundaries.

2.1.1 Physical Model Configuration and Forcing

The HIC6k hindcast is implemented using the Modular Ocean Model version 6 (MOM6; Adcroft et al., 2019), a finite-volume numerical ocean model. The HIC6k model domain (Fig. 1) is designed to cover both the Southeast (windward) and Northwest (leeward) regions of the Hawaiian Island Chain, including the

https://doi.org/10.5194/egusphere-2026-1877
Preprint. Discussion started: 29 July 2026

Papahānaumokuākea Marine National Monument. It also covers the surrounding regions of the southeastern portion of the NPSG, including the primary bigeye tuna fishing grounds off Hawai‘i, which stretch from the dateline to 120°W and from equatorial waters to roughly 40°N, following the fleet's documented expansion over the past two decades (Woodworth-Jefcoats et al., 2018).

In the vertical dimension, the HIC6k configuration uses 75 layers using a z* coordinate system. Rather than confining sea surface height variations to the top layer, these coordinates stretch and compress all water-column layers proportionally to mirror changes in sea level (Adcroft, A. & Campin, 2004). A minimum bathymetric depth of 5 m is imposed. The grid is structured to maintain a uniform 2 m resolution throughout the uppermost 8 m, after which layer thickness stretches monotonically with depth, transitioning smoothly from ~ 2 m near the surface to a maximum of 250 m across the lower water column. To maximize computational efficiency, model integrations employ split time-stepping between physical dynamics and passive tracers. Fluid dynamics are resolved using a baroclinic time step of 300 seconds alongside an adaptive, stability-constrained barotropic step (Hallberg, 1997; Hallberg and Adcroft, 2009). Thermodynamics and biogeochemical processes, which tend to evolve more slowly than the dynamic ones, were updated less frequently, using a 900 second time step. The longer time step should have little effect on the representation of the mesoscale, but may not fully resolve rapid thermodynamic variability driven by baroclinic tides and internal waves in topographically complex regions.

The schemes and settings used for the physical model simulation are largely consistent with those used by Ross et al. (2023) in the Northwest Atlantic. A full account of the parameterization choices implemented for the simulations presented in this study can be found in the supplemental material (MOM_parameter_doc.all). A number of region-specific adjustments, however, were implemented to improve performance. These will be summarized in Section 2.2.

The 31-year ocean hindcast simulation (1993-2023) was run on the National Climate-Computing Research Center’s high-performance computing system, GAEA. Atmospheric forcing was applied at hourly intervals using the ECMWF Reanalysis 5 dataset (ERA5; Hersbach et al., 2020). After re-scaling variables to the standard 2 m reference height, surface wind stress alongside latent and sensible heat fluxes were computed using Large and Yeager’s (2004) bulk formulations. We computed light attenuation through the water column using prognostic chlorophyll from the biogeochemical model, following the approach of Manizza et al. (2005), with parameters optimized for light attenuation in the NPSG (see Section 2.2).

Temperature, salinity, sea surface height, and momentum at the open lateral boundaries, along with the initial conditions, were derived from daily-averaged output of the 1/12° Global Ocean Physics Reanalysis (GLORYS12; Lellouche et al., 2021). Boundary tidal forcing was specified using amplitude and phase information from the TPXO Global tidal elevation and transport atlas, version 9 (Egbert and Erofeeva, 2002), following the tidal implementation of Ross et al. (2023) and Drenkard et al. (2025). This included the four principal semidiurnal constituents (M2, S2, N2, K2), four diurnal constituents (K1, O1, P1, Q1), and two long-period constituents (Mm, Mf). All initial and boundary fields were interpolated onto the HIC6k grid using the xesmf regridding package (Zhuang et al., 2023). As in Ross et al. (2023) and Drenkard et al. (2025), boundary conditions were applied using a Flather (1976) scheme for barotropic flow and an Orlanski (1976) radiation condition for baroclinic flow.

A lateral transition zone separates the high-resolution interior and parent-domain boundaries. Within the zone, the horizontal grid spacing increases from the 6 km interior to 12 km at the boundary and a damping sponge relaxes horizontal momentum (u, v) and tracers (temperature and salinity) toward monthly mean fields from the parent-domain reanalysis. Damping is applied using spatially varying relaxation timescales that strengthen toward the boundary edge to a minimum of 10 days. The width of the transition zone is defined in physical space (three first-mode baroclinic Rossby radii) to ensure that mesoscale features experience damping over a distance comparable to their intrinsic horizontal scale. This approach provides continuous moderate relaxation that ensures

https://doi.org/10.5194/egusphere-2026-1877
Preprint. Discussion started: 29 July 2026

smooth transitions between the regional domain and the global ocean state while preserving mesoscale features and island-modified circulation patterns within the interior domain.

2.1.2 Biogeochemical Model Configuration and Forcing

Ocean biogeochemistry is simulated using the Carbon, Ocean Biogeochemistry and Lower Trophics model, version 3.0 (COBALTv3.0; Stock et al., 2020, 2025), which resolves 40 prognostic state variables representing plankton food-web dynamics and the cycling of carbon, nitrogen, phosphorus, iron, silica, calcium carbonate, and lithogenic material across open-ocean and coastal environments. This version, also used by Ross et al. (2023) and Drenkard et al. (2025), extends prior COBALT formulations (Stock et al., 2014, 2020) through the addition of a third phytoplankton size class (following Van Oostende et al., 2018), more flexible zooplankton feeding, direct phytoplankton sinking, and improved phytoplankton photoadaptation and photoacclimation dynamics (Stock et al., 2025). It also incorporates a modified version of the dynamic N:P stoichiometry scheme of Galbraith and Martiny (2015), first implemented within COBALT by Ross et al. (2023). The stoichiometric parameters used in that earlier implementation, however, required adjustment for this region to appropriately represent NPSG conditions (see Section 2.2).

Initial and boundary conditions for the major macronutrients NO_3, SiO_4, O_2 and Fe were derived from the 2018 World Ocean Atlas. We applied seasonal climatologies for depths above 800 m where seasonal data are available in WOA, and annual climatologies at greater depths where WOA provides only long-term means (de Boyer et al., 2019; García et al., 2019a,b) similar to the implementations in Ross et al. (2023) and Drenkard et al. (2025). For PO_4, annual climatologies were obtained from GLODAP to better represent the naturally lower phosphate concentrations observed in this region (Martiny et al., 2019). Initial and boundary conditions for biological tracers beyond macronutrients, which equilibrate rapidly to ambient nutrient and light conditions, were initialized from a global ¼° OM4p25 simulation using COBALTv3 (similar to Liu et al., 2021). We note that this data-driven approach for macronutrients and oxygen, which is common in regional biogeochemical simulations, minimizes biases relative to forcing with a global biogeochemical simulation, but it may also dampen variability arising from climate-driven nutrient anomalies. This choice will be discussed in Section 4. Dissolved inorganic carbon (DIC), which has a strong anthropogenic trend, was set using the Empirical Seawater Property Estimation Routines (ESPER) presented by Carter et al. (2021). ESPER was also used to specify the alkalinity. Riverine output is not prescribed in this model as the Hawaiian Islands lack any major river system.

2.2 Model Adjustments for the NPSG

The base implementation of the physical and biogeochemical model components following Ross et al. (2023) was modified in several ways to improve performance in the NPSG environment. These are described in the subsections below.

2.2.1 Reduced Blue-Green Light Attenuation

Similar to the findings of Friedrich et al. (2024), modeling light propagation through the water column from the Manizza et al. (2005) scheme with parameters described therein resulted in over-attenuation of radiation relative to measurements at Station ALOHA. We thus calibrated the blue/green light attenuation coefficient to Station ALOHA data. This resulted in a clear water blue attenuation coefficient parameter (ksw) of 0.018 m^{-1}, consistent with the most penetrating wavelengths in clear, case I waters (Morel et al., 1988) and significantly lower than the default Manizza value of 0.0232 m-1, which was an average over a broader set of blue-green wavelength bands. This change produces an attenuation that also matches the long-term data of the Hawaiian Ocean Time-series (HOT) program at Station ALOHA, resulting in more blue-green light energy at deeper layers of the euphotic zone. In more

https://doi.org/10.5194/egusphere-2026-1877
Preprint. Discussion started: 29 July 2026

productive waters, attenuation in the Manizza scheme is strongly controlled by chlorophyll, so this change has little impact on attenuation around the MHI and in other areas with elevated productivity.

2.2.2 Increased Background Vertical Diffusion and Gustiness

The NPSG is highly stratified, often characterized as a two-layer structure. In initial simulations, we found near-surface stratification was excessive, particularly in low wind conditions during summer months, and resulted in concentrated temperature and salinity biases just below the mixed-layer. Two adjustments to the model configuration were employed to address this:

1.) The background vertical diffusion coefficient (KD), which ensures a minimum level of vertical mixing throughout the water column, was increased by an order of magnitude (from 1×10^{-6} to 1×10^{-5} m²/s). In MOM6, background diffusivity represents small-scale turbulent processes in the ocean interior. A background value of 1×10^{-5} m²/s remains orders of magnitude below typical vertical diffusion rates in moderately and vigorously mixed systems (~1×10^{-4} - 1×10^{-2} m²/s).
2.) A gustiness parameter of 0.017 m/s was employed. The gustiness parameter is a small background wind velocity - representing atmospheric variability, such as convective gusts and small scale turbulence, unresolved in the atmospheric forcing - is added in quadrature to the resolved wind speed when computing wind stress. The resulting effective wind speed maintains a minimum level of shear and turbulence at the ocean surface during low winds.

With increased exchange of tracer and momentum properties between model layers, simulations demonstrated a smoother transition between the mixed layer and water below more similar to that shown in observations. Application of the gustiness parameter resulted in mixed layer depths that more closely matched observations. In combination, the adjustments improved the representation of mixed layer dynamics and removed bias errors found in earlier model runs.

2.2.3 Targeted Longwave Radiation Calibration

To address energetic imbalances between the atmospheric forcing and ocean model components, we applied a spatially-targeted 10% increase to the downwelling longwave radiation from ERA5, with the adjustment focused along 30°N where the model exhibited excessive cooling. This adjustment was not intended to correct deficiencies in the ERA5 reanalysis itself, but rather to account for inconsistencies arising from the use of incompatible ocean boundary conditions. While ERA5 uses a simple ocean model to maintain this balance, GLORYS12 employs data assimilation that effectively adjusts the atmospheric forcing to better represent the ocean state. However, these assimilation-driven adjustments are not publicly available. Consequently, our MOM6-integrated ocean, conditioned by GLORYS12 boundary conditions, is no longer consistent with the original, unperturbed ERA5 atmospheric forcing. This mismatch creates a persistent radiative imbalance as GLORYS12-conditioned waters continue to be introduced at the open boundaries, necessitating the longwave radiation adjustment to restore energetic equilibrium. This correction reduced the domain-mean SST cold bias relative to GLORYS12 by 37% (from -0.41ºC to -0.26ºC) and eliminated the persistent negative ocean heat drift present in the uncorrected simulation.

2.2.4 Wind Current Feedbacks

During initial validation of the HIC6k, we identified a systematic underestimation of EKE by approximately 40% compared to satellite altimetry (AVISO) and 23% compared the ocean reanalysis (GLORYS12) (Fig. S2). Following Renault et al. (2016, 2019), we traced this bias to the over-correction of current feedback effects in the surface wind stress formulation. The issue arises because atmospheric reanalysis products (e.g. ERA5) inherently include current feedback effects through data assimilation over the real ocean. When ocean-only models calculate relative wind

https://doi.org/10.5194/egusphere-2026-1877
Preprint. Discussion started: 29 July 2026

stress using the velocity difference between winds and ocean surface currents ($u_{diff} = u_{surf} - u_{atm}$, $v_{diff} = v_{surf} - v_{atm}$), current feedback is accounted for twice, resulting in excessive damping of mesoscale eddies. In Figure 11 of Renault et al. (2019), they explicitly identify this problem in their decision tree for proper current feedback treatment across different modeling configurations.

To address this, we modified the FMS coupler (surface_flux.F90) to include a tunable current feedback scaling parameter (α_{cfb}):

$$u_{diff} = \alpha_{cfb} * u_{surf} - u_{atm}$$

$$v_{diff} = \alpha_{cfb} * v_{surf} - v_{atm}$$

Where u_{surf} and v_{surf} are ocean surface currents, and u_{atm} and v_{atm} are atmospheric winds. The parameter α_{cfb} controls current feedback strength, ranging from 0.0 (absolute wind stress, no additional feedback) (Fig. S1 j-l) to 1.0 (full relative wind formulation) (Fig. S1 a-c). For the HIC6k simulation, we calibrated α_{cfb}= 0.2 through comparison with GLORYS12 reanalysis and AVISO altimetry, achieving optimal representation of mesoscale eddy activity (Fig. S1 g-i). This intermediate value accounts for the particle current feedback already present in ERA5 reanalysis while allowing some additional current feedback needed to improve mesoscale variability in the simulation.

2.2.5 Calibration of Phytoplankton Phosphorous to Nitrogen ratios

While the NPSG is generally nitrogen limited, the phytoplankton community also reduces phosphorus to very low levels. This has been attributed to the combined influence of diazotrophs, which act to weaken N relative to P limitation through nitrogen fixation, and general flexibility in P-quotas within the phytoplankton community (Martiny et al., 2019, Moreno and Martiny 2018). COBALTv3 includes both a diazotroph group and a simple representation of P usage flexibility following the "Line of Frugality" (LoF) concept introduced by Galbraith and Martiny (2015). The LoF approximates the relationship between P:C ratios and ambient P concentrations as a linear empirical relationship whereby P:C ratios increase with more P. This relationship, however, is an emergent pattern reflecting several underlying mechanisms (Moreno and Martiny 2018) and has considerable uncertainty and unexplained variability.

Prior implementations of COBALTv3 (e.g., Ross et al., 2023; Drenkard et al., 2025) used the steeper of two lines of frugality proposed by Galbraith and Martiny (2015) and applied a fixed P:N of 1:40 to diazotrophs. This steep LoF helped ensure full usage of N in prominent low P:N river inputs in these systems (e.g., the Mississippi River), as observed. These settings, however, left too much P in surface NPSG waters. We utilized the shallower of the LoF slopes presented by Galbraith and Martiny (2015) for the simulations herein and extended its application to diazotrophs. Details of the stoichiometry settings are provided in Table S1 and sensitivity will be presented in the Results.

These modifications reflect the natural phosphorus plasticity observed in marine phytoplankton, allowing for enhanced phosphate uptake and sequestration from the water column, thereby reducing the persistent positive phosphate bias in our model while maintaining mechanistically consistent stoichiometric relationships.

2.3 Observational Datasets

We evaluated HIC6k performance against a comprehensive suite of observational products spanning basin-scale to nearshore spatial scales and seasonal to interannual temporal scales. This multi-scale evaluation strategy reflects

https://doi.org/10.5194/egusphere-2026-1877
Preprint. Discussion started: 29 July 2026

three marine-resource focused evaluation objectives: (1) basin-scale pelagic habitat dynamics, (2) island-ocean interactions and mesoscale biological productivity, and (3) coastal temperature variability.

2.3.1 Basin-Scale Gridded Products

We compared model output against two complementary ocean reanalysis products that provide basin-scale context for evaluating temperature gradients, frontal zones, and seasonal variability relevant to pelagic fish habitat. GLORYS12 (Lellouche et al., 2021) is a global eddying (1/12° resolution) data-assimilative ocean reanalysis that assimilates satellite altimetry, sea surface temperature, and in-situ temperature and salinity profiles to produce dynamically consistent 3D physical ocean state estimates. OISST version 2.1 (Huang et al., 2021) is generated from multiple satellite and in-situ temperature data sources and interpolated to a 1/4° global grid, providing daily sea surface temperature fields. Both products have continuous monthly output covering 1993-2023, enabling evaluation of interannual variability and long-term mean conditions. Because our model's initial and boundary conditions are derived from GLORYS12, comparing against GLORYS12 does not represent independent validation but rather quantifies how MOM6's internal dynamics deviate from the parent reanalysis over time. GLORYS12 thus serves as a consistency benchmark for 3D structure including thermocline depth distributions critical for habitat compression assessments, while OISST provides a satellite-based surface temperature reference for identifying frontal boundaries and model skill.

Surface chlorophyll concentrations were compared against the European Space Agency's Ocean Color Climate Change Initiative product (OC-CCI; Sathyendranath et al., 2019, 2023), which merges multiple satellite ocean color sensors to provide consistent long-term records. Monthly OC-CCI chlorophyll-a fields from 1998-2019 were remapped from 4 km native resolution to the HIC6k grid. These data are used as a proxy for phytoplankton biomass and enable evaluation of its patterns within the central portion of the NPSG and assessment of oligotrophic baseline conditions that influence forage base availability for pelagic predators.

We validated the mixed layer depth (MLD) from HIC6k against the 1° monthly MLD climatology developed by de Boyer Montégut (2024). This climatology uses an assemblage of MBT, XBT, and CTD casts and profiling floats, defining the MLD as the depth where the potential density is 0.03 kg m^{-3} greater than the density at a 5 m reference depth. To maintain consistency with de Boyer Montégut, we utilized the diagnostic variable MLD_003 from the HIC6k MOM6 output. This variable defines the MLD as the depth at which the potential density increases by 0.03 kg m^{-3} relative to a user-defined surface reference depth, which was set to 5 m in this study.

Climatological mean distributions of surface and subsurface macronutrient (NO_3, PO_4) and oxygen concentrations were compared against the 2023 World Ocean Atlas (WOA23; Garcia et al., 2023a,b) for the period 1993-2023. WOA provides objectively analyzed climatological fields at 1° resolution derived from quality-controlled in-situ profile data. We used WOA to assess the model's representation of basin-scale spatial patterns in the meridional nutrient gradients that structure productivity patterns across the North Pacific. The climatological nature of WOA makes it particularly suited for evaluating long-term mean states rather than interannual variability.

We evaluated the model's temporal variability in oxygen distributions using the Gridded Ocean Biogeochemistry from Artificial Intelligence (GOBAI) oxygen product (Sharp et al., 2023). GOBAI-O_2 provides monthly gridded fields of dissolved oxygen on a 1° × 1° grid from 2004-2022, derived from Argo float oxygen measurements using machine learning algorithms. The product uses a neural network trained on quality-controlled Argo-O_2 observations to map oxygen concentrations throughout the upper 2000 m of the global ocean. For comparison with the model, we extracted oxycline depth time series along 150°W, defining oxycline depth as the depth of the 70 μmol kg^{-1} oxygen isoline, consistent with our model analysis (see Section 3.1). The GOBAI-O_2 product provides independent validation of interannual oxygen variability, complementing the climatological World Ocean Atlas fields used for mean state assessment.

https://doi.org/10.5194/egusphere-2026-1877
Preprint. Discussion started: 29 July 2026

2.3.2 Mesoscale observations for Island wakes assessment

Geostrophic currents derived from satellite altimetry (AVISO, 2023) were used to evaluate mesoscale eddy characteristics that modulate biological productivity in island wakes and the broader Pacific Islands region. Specifically, we assessed eddy kinetic energy distributions, eddy size characteristics, and propagation patterns. Altimetry provides independent observation of sea surface height variability that directly constrains mesoscale circulation features critical for nutrient transport to oligotrophic surface waters and the formation of biological hotspots downstream of islands.

The OC-CCI chlorophyll product also serves to evaluate the model's representation of island mass effects (De Falco, et al., 2022), the enhanced biological productivity observed in island lee regions and extending downstream in island wakes. These features represent critical foraging grounds for pelagic predators and seabirds in otherwise oligotrophic waters.

2.3.3 In-Situ Observations

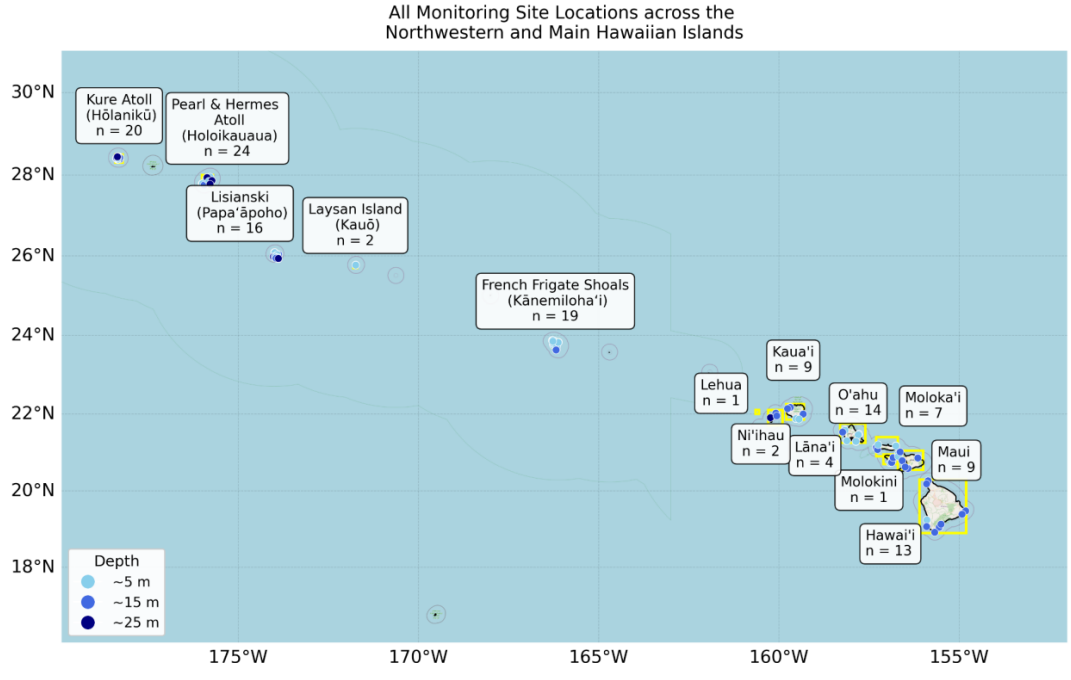

Figure 2. Spatial distribution of coral reef temperature monitoring sites across the Northwestern Hawaiian Islands and Main Hawaiian Islands used for model–observation comparisons. Circles indicate the locations of subsurface temperature recorders (STRs) deployed by NOAA's Pacific Islands Fisheries Science Center at 141 coral reef sites spanning the full Hawaiian Archipelago, including Kure Atoll, Pearl and Hermes Atoll, Lisianski, Laysan Island, French Frigate Shoals, Lehua, Niʻihau, Kauaʻi, Oʻahu, Molokaʻi, Lānaʻi, Molokini, Maui, and Hawaiʻi. STRs were deployed at nominal depths of ~5 m, ~15 m, and ~25 m (light blue, medium blue, and dark blue, respectively), as part of NOAA's National Coral Reef Monitoring Program (NCRMP). In situ temperature records from these sites were used to evaluate modeled sea surface and subsurface temperatures across reef environments.

https://doi.org/10.5194/egusphere-2026-1877
Preprint. Discussion started: 29 July 2026

Station ALOHA (22.75°N, 158°W) is the primary sampling site for the Hawaiian Ocean Time-series (HOT) program, which has provided nearly three decades of monthly hydrographic, biogeochemical, and ecological measurements in the NPSG (Karl and Lukas, 1996). We utilized HOT measurements of temperature, salinity, dissolved oxygen, inorganic nutrients (nitrate, phosphate, silicate), dissolved inorganic carbon, total alkalinity, pH, and chlorophyll profiles, binned onto the model's native vertical grid over the upper 1000 m, to evaluate the model's representation of oligotrophic gyre biogeochemistry. We also compare fluxes and biomass pools from the plankton food web against measurements derived from various targeted studies conducted at HOT. The long-term nature of this time series enables assessment of seasonal cycles, interannual variability, and mean state conditions in the baseline oligotrophic environment that characterizes much of the modeled domain. Station ALOHA serves as a critical validation point for biogeochemical model performance, as accurate representation of nutrient-limited productivity and carbonate chemistry in oligotrophic waters underpins the model's utility for ecosystem applications.

The global Argo array (Roemmich et al., 2009) provides vertically-resolved temperature and salinity profiles with near-global coverage. We used Argo data to assess the model's representation of upper ocean thermal structure relevant to pelagic habitat, including thermocline depth (critical for defining vertical habitat boundaries), mixed layer depth variability (influencing prey availability), and vertical temperature gradients across the model domain. The spatial distribution of Argo profiles enables evaluation of basin-scale patterns in vertical structure that control the depth ranges accessible to pelagic predators. Argo profiles were interpolated onto the model’s native vertical grid for comparison with model output.

Nearshore temperature validation utilized the NOAA Pacific Islands Fisheries Science Center's network of subsurface temperature recorders (STRs) deployed at 141 coral reef monitoring sites (Fig. 2) across the Hawaiian archipelago, including Hawai‘i, Maui, O‘ahu, Kaua‘i, Moloka‘i, Lāna‘i, Ni‘ihau, Molokini, Lehua, French Frigate Shoals, Laysan, Lisianski, Pearl and Hermes Atoll, and Kure (Smith and Barkley, 2025; Perelman et al., 2024). STRs (SeaBird Electronics SBE-56) were deployed at depths of 5, 15, and 25 m, corresponding to shallow, mid, and deep reef strata as part of NOAA’s National Coral Reef Monitoring Program (NCRMP). Temperature was recorded hourly with instrument servicing and redeployment occurring approximately every three years between 2010 and 2019. These data directly address the third evaluation objective by providing high-temporal-resolution subsurface temperatures at coastal observing stations designed to characterize reef habitat conditions. Unlike satellite-based sea surface temperature products, STR measurements capture temperatures at depths where corals experience thermal stress, making them the most appropriate validation dataset for assessing whether the model can capture time-varying hydrographic anomalies relevant to coral bleaching risk. To assess spatial variation in model performance, monitoring sites were grouped by their nearest island (Hawai‘i, Maui, O‘ahu, Kaua‘i, Moloka‘i, Lāna‘i, Ni‘ihau, Molokini, Lehua, French Frigate Shoals, Laysan, Lisianski, Pearl and Hermes Atoll, and Kure), and correlations between observed and modeled temperatures were calculated separately for each island group. The temporal resolution (hourly) and multi-year deployment periods enable evaluation of the model's capacity to resolve both synoptic-scale temperature events (days to weeks) and seasonal to interannual variability (months to years) critical for coral thermal exposure variability.

These in-situ subsurface measurements were complemented by NOAA Coral Reef Watch's daily global 5 km CoralTemp sea surface temperature product (version 3.1; Liu et al., 2014; Skirving et al., 2020). CoralTemp is specifically designed for coral reef thermal stress monitoring and uses nighttime-only satellite observations to avoid daytime heating biases, providing 0.05° resolution SST estimates from 1985-present. This product is currently used operationally by NOAA for coral bleaching heat stress alerts and provides finer spatial resolution (5 km) than OISST (25 km), enabling better characterization of nearshore thermal gradients in reef-influenced coastal zones. Daily CoralTemp SST data covering 1993-2023 were used to assess the model's representation of surface temperature variability surrounding the Hawaiian Islands, providing a satellite-based surface complement to the subsurface STR measurements at reef monitoring depths.

https://doi.org/10.5194/egusphere-2026-1877
Preprint. Discussion started: 29 July 2026

2.3.4 Validation Strategy

This observational framework enables hierarchical validation aligned with the three primary model evaluation objectives. Basin-scale products (WOA climatologies, reanalysis, satellite SST, deBoyer MLD, ocean color, and Argo floats) assess whether the model accurately resolves pelagic habitat dynamics including temperature gradients, frontal zones, oxycline structure, and plankton productivity patterns. In-situ observations at Station ALOHA provide detailed validation of oligotrophic gyre biogeochemistry, characterizing the baseline nutrient-limited conditions that prevail across much of the Pacific Islands region. Mesoscale observations (altimetry, ocean color) evaluate the model's representation of island-ocean interactions and the biological hotspots created in island wakes. Coastal observations (NCRMP STR network) determine whether the model provides sufficient resolution for nearshore applications, specifically the capacity to capture time-varying hydrographic anomalies at reef monitoring stations. The combination of climatological products (spatial patterns), satellite products (spatial coverage and temporal evolution), moored time series (temporal resolution and biogeochemical detail), profiling floats (3D structure), and coastal sensors (nearshore reef conditions) provides comprehensive assessment across the spatial scales and environmental variables critical for marine resource management applications in the Central North Pacific region.

3. Results

3.1 Basin-Scale Physical Dynamics

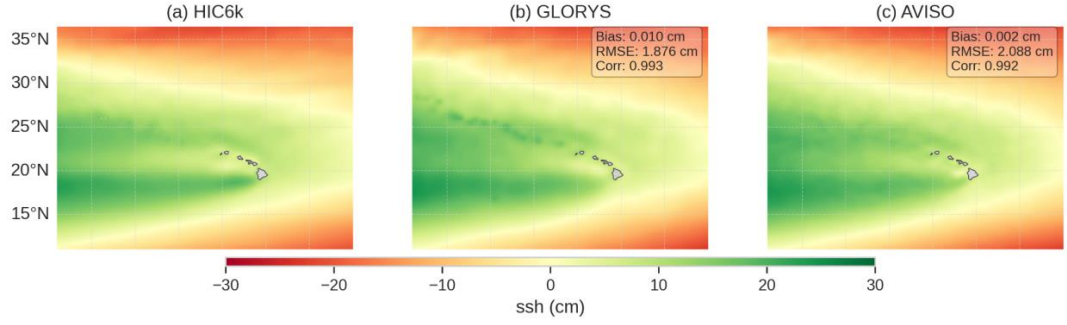

Figure 3. Comparison of sea surface height (SSH) spatial anomalies (removal of the spatial mean at each time step (1993-2023)) from (a) HIC6k, (b) GLORYS12, and (c) AVISO.

The model reproduces the fundamental physical structure and variability in the North Pacific Ocean. Sea surface height (SSH) spatial anomaly comparisons with AVISO altimetry and GLORYS12 reanalysis reveal that the model captures the broad meridional gradient and general spatial structure of SSH anomalies (Fig. 3). Both model and observational datasets show the transition from negative anomalies in the northern portion (~30-35°N) to positive anomalies in the southern region (~15-20°N), representing the mean large-scale pressure gradients that drive geostrophic circulation patterns in this region.

https://doi.org/10.5194/egusphere-2026-1877
Preprint. Discussion started: 29 July 2026

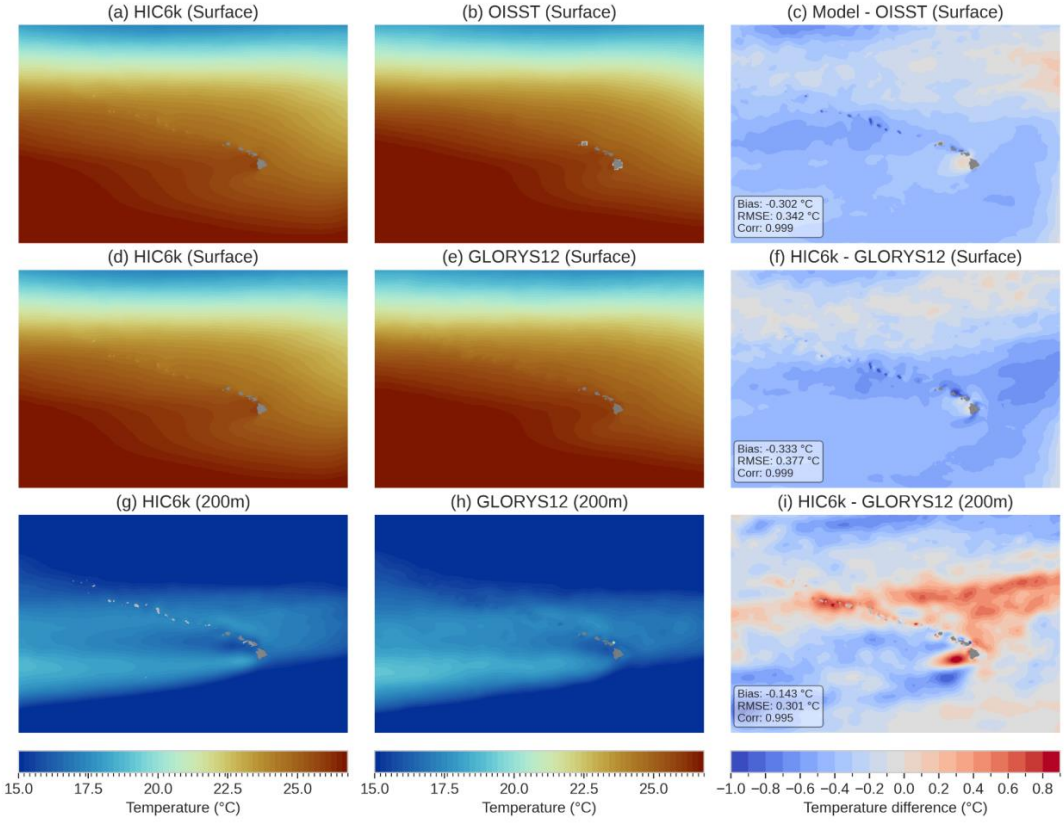

Figure 4. Comparison of sea surface and subsurface temperature between surface temperatures from (a) HIC6k, (b) OISST, and (c) their difference; (d) HIC6k, (e) GLORYS12, and (f) their difference; and 200m depth temperatures from (g) HIC6k, (h) GLORYS12, and (i) their difference. Statistics in difference panels show bias, RMSE, and correlation coefficient.

This realistic circulation is supported by accurate temperature and salinity distributions throughout the upper ocean. The model captures annual mean temperature and salinity patterns in the upper ocean (0-200m; Fig. 4-5). Temperatures generally fall within ~0.5°C of OISST across the open ocean domain (surface RMSE = 0.34°C; Fig. 4c) and are consistent with GLORYS12 SST values (surface RMSE = 0.38°C; 200m RMSE = 0.30°C; Fig. 4f,i). The model successfully reproduces the pronounced poleward cooling of surface waters at the NPTZ at approximately 30°N. The model also captures the seasonal migration of this frontal feature, with the mean latitude of the 18ºC (64.4ºF) isotherm varying consistently with OISST observations (r=0.97; Fig. S2), including both the amplitude (~10º latitude) and timing of the annual cycle.

https://doi.org/10.5194/egusphere-2026-1877
Preprint. Discussion started: 29 July 2026

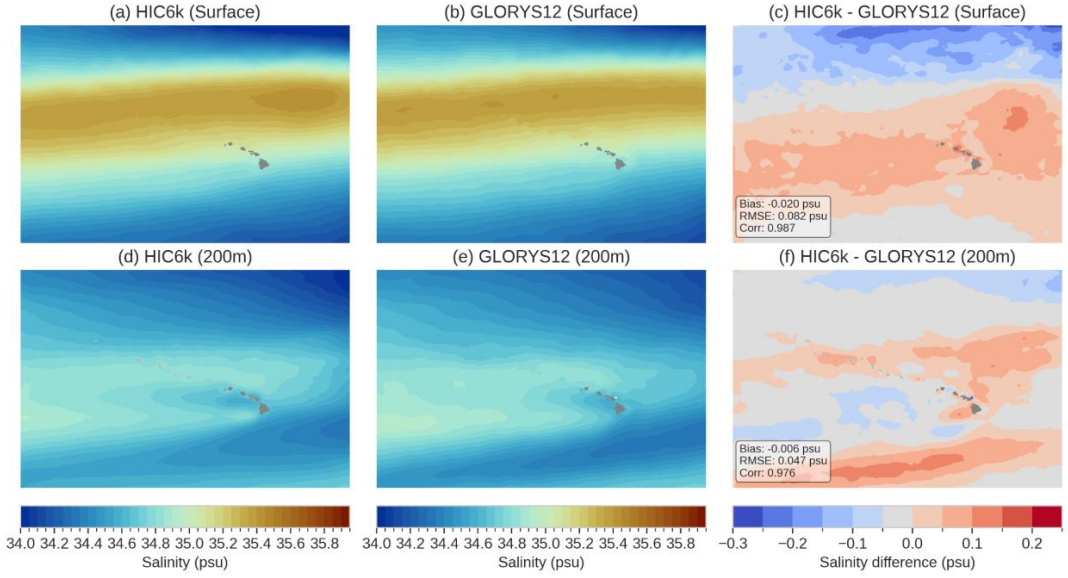

Figure 5. Comparison of sea surface and subsurface salinity (psu) between surface salinity from (a) HIC6k, (b) GLORYS, and (c) their difference, and 200m depth salinity from (d) HIC6k, (e) GLORYS12, and (f) their difference. Statistics in difference panels show bias, RMSE, and correlation coefficient.

Salinity distributions show similarly strong correspondence with observations, capturing the basin-scale meridional gradient with biases remaining below ±0.2 psu across most of the open ocean domain (surface RMSE = 0.08 psu, decreasing to 0.04 psu at 200 m), with localized exceptions reaching ±0.3 psu (Fig. 5). The model exhibits slightly fresher conditions near the northern and southern boundaries and marginally elevated salinity in the subtropical interior, suggesting a somewhat stronger meridional gradient than GLORYS12. This subtle bias persists to 200 m depth, though the overall trend toward less saline water with depth in the central NPSG is well captured.

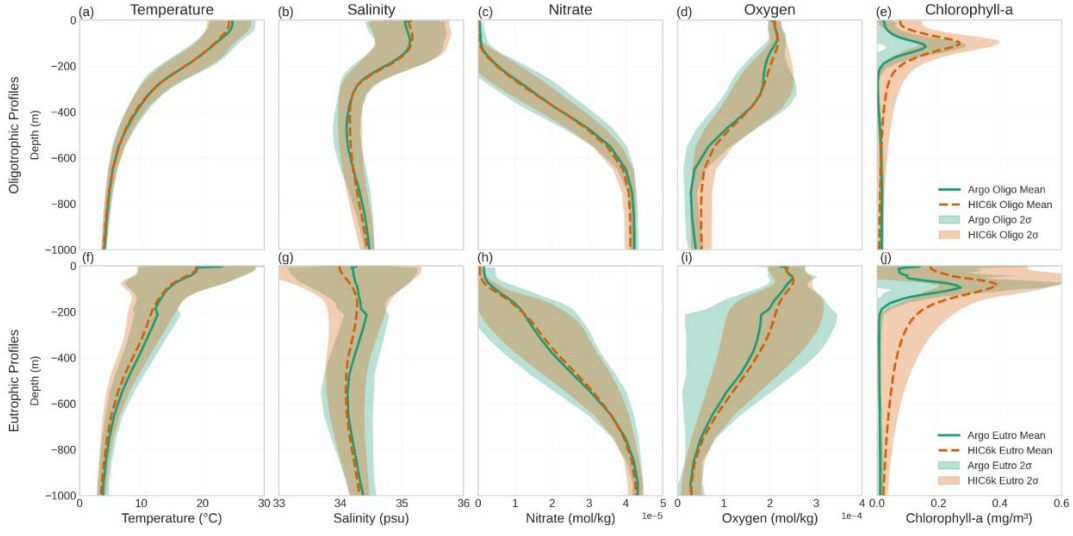

https://doi.org/10.5194/egusphere-2026-1877
Preprint. Discussion started: 29 July 2026

Figure 6. Argo vertical profiles of oceanographic and biogeochemical properties. Mean profiles (0-1000 m depth) of temperature, salinity, nitrate, dissolved oxygen, and chlorophyll-a for (top row) argo floats in oligotrophic regions (Chlorophyll-a < 0.135mgChl/m^3), and (bottom row) eutrophic regions (Chlorophyll-a > 0.135mgChl/m^3). Each panel compares Argo observations (green line), model output from HIC6k (dashed orange line), with 2σ uncertainty bounds (shaded region green and orange respectively).

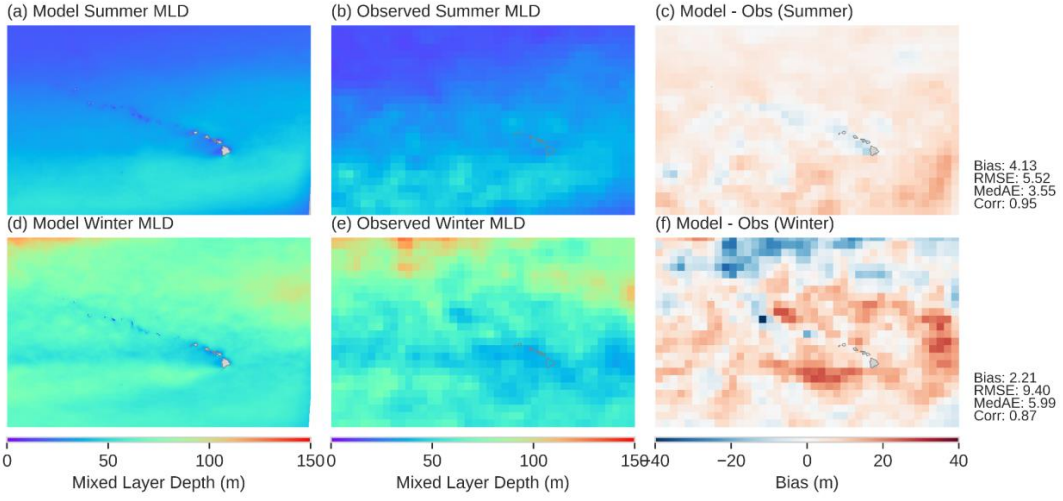

Figure 7. Comparison of seasonal mixed layer depth (MLD) between model and observations. Summer MLD from (a) HIC6k, (b) Argo-based observations (de Boyer Montégut climatology), and (c) their difference (Model - Obs); Winter MLD from (d) HIC6k, (e) Argo observations, and (f) their difference. Difference panels show bias, RMSE, median absolute error (MedAE), and spatial correlation coefficient.

Basin-wide Argo profile comparisons reveal that the model successfully captures thermocline and halocline structure throughout the upper 1000m for both oligotrophic and eutrophic regions (Fig. 6). Temperature profiles closely follow observed medians from surface to depth, while salinity profiles reproduce the subsurface salinity maximum near 200 m. The simulation captures both the primary differences between seasons (Fig. 7 a-c versus Fig. 7d-e) and the primary spatial contrasts in mixing depth within each season (r = 0.95 in summer, r = 0.87 in winter). The model shows a modest positive bias in mixed layer depth of ~5m during both seasons, though this is comparable to observational and computational uncertainties.

https://doi.org/10.5194/egusphere-2026-1877
Preprint. Discussion started: 29 July 2026

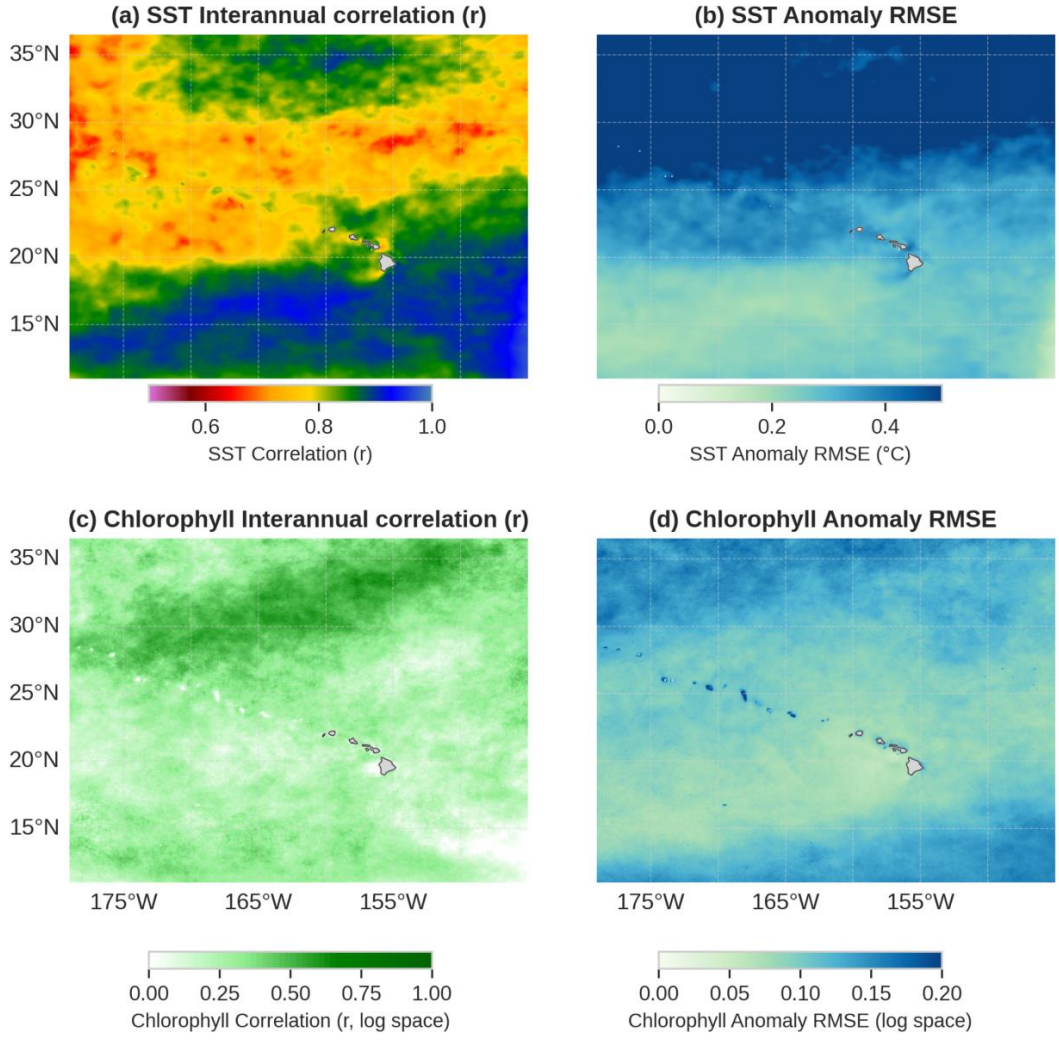

Figure 8. Spatial patterns of Interannual correlation (left) and anomaly RMSE (right) for **(a,b) sea surface temperature vs. OISST (1993-2023) and (c,d) surface chlorophyll vs. OC-CCI (September 1997-December 2023)**. Metrics computed on deseasonalized monthly anomalies (climatological monthly means removed at each grid point). Chlorophyll analyzed in $\log_{10}$ space.

The model reproduces both the mean state and interannual SST variability across the basin, with temporal correlations exceeding 0.95 throughout most of the domain and reaching $r > 0.96$ in the central and eastern portions of the domain (Fig. 8a). Root mean square errors remain low (<0.5°C) across the subtropical gyre, increasing modestly (~0.6-0.7°C) only in western boundary current regions and coastal zones where mesoscale activity intensifies (Fig. 8b).

3.2 Basin-scale Biogeochemical dynamics

https://doi.org/10.5194/egusphere-2026-1877
Preprint. Discussion started: 29 July 2026

The model reproduces vertical biogeochemical structure in both oligotrophic and eutrophic waters. Argo profile comparisons show that the model captures vertical distributions of nitrate and dissolved oxygen throughout the upper 1000m in both oligotrophic (chlorophyll-a < 0.135 mg/m³) and eutrophic (chlorophyll-a > 0.135 mg/m³) waters (Fig. 6), with model profiles generally falling within 2σ observational uncertainty bounds. The model reproduces key features including the nutricline structure and oxygen minimum zone characteristics. Chlorophyll-a profiles capture the deep chlorophyll maximum (DCM) structure in both regimes, though in eutrophic waters the model maintains elevated chlorophyll concentrations at depth (below ~100m) while observations show a sharper decline (Fig. 6e,j).

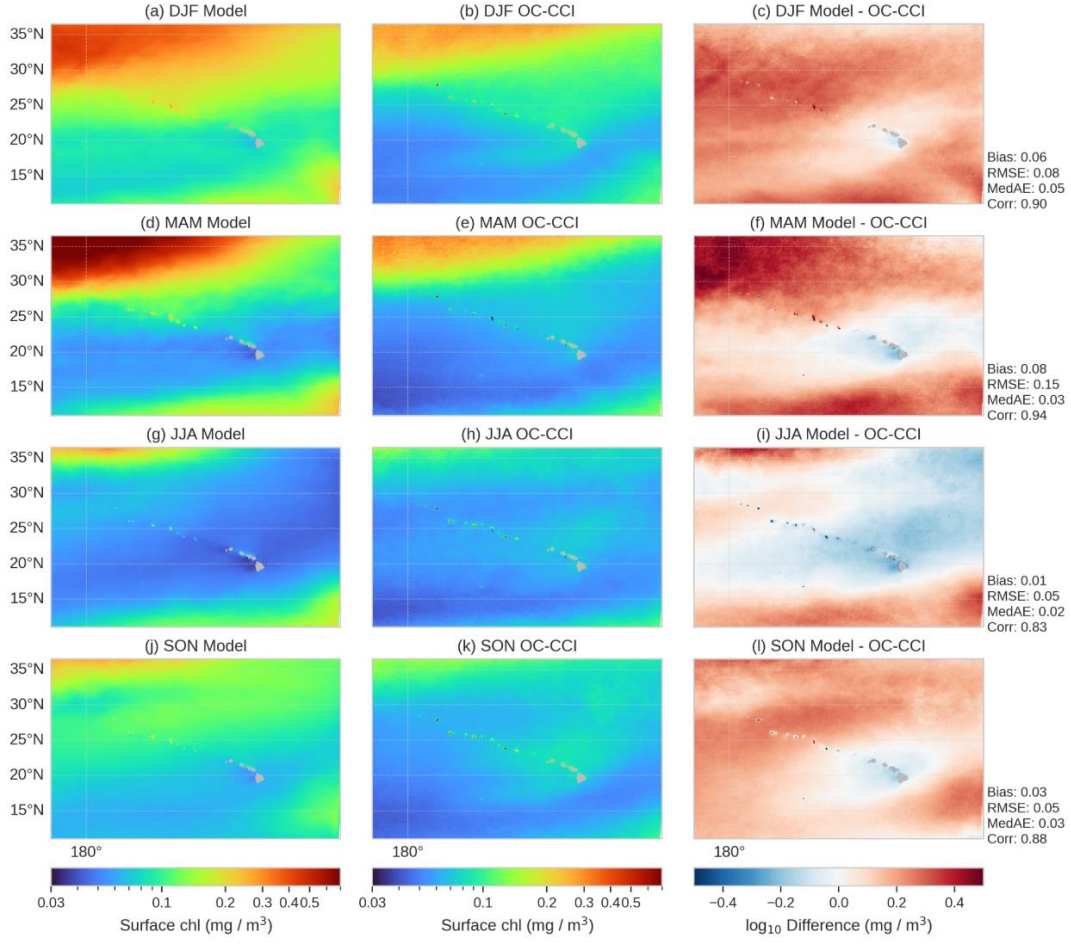

Figure 9. Seasonal comparison of surface Chl-a concentrations between model and satellite observations. HIC6k (left column), OC-CCI satellite observations (middle column), and their difference (Model - OC-CCI, right column) for (a-c) Winter (DJF), (d-f) Spring(MAM), (g-i) Summer(JJA), and (j-l) Fall (SON). Difference panels show bias, RMSE, median absolute error (MedAE), and spatial correlation coefficient. As described in Section 2, bias, RMSE and MedAE are calculated on $\log_{10}$-transformed data, so a difference of 0.3 corresponds to a factor of 2 discrepancy between the model and satellite-based estimate.

https://doi.org/10.5194/egusphere-2026-1877
Preprint. Discussion started: 29 July 2026

The model reproduces both the spatial distribution and seasonal variability of surface chlorophyll across the subtropical North Pacific high seas (Fig. 9). The model captures the transition from oligotrophic subtropical waters (<0.2 mg/m³) to more productive waters along the northern boundary of the domain, with this gradient migrating seasonally. During winter (DJF), both model and OC-CCI satellite data show the TZCF positioned near its southern extent around 30-35°N, marking the boundary between the nutrient-depleted subtropical gyre and the nutrient-enriched transition zone. In spring (MAM), the productive zone shifts northward, though the model shows increased spatial variability during this transitional period. By summer (JJA), the domain exhibits uniformly low chlorophyll concentrations as the productive boundary migrates beyond the northern extent. Fall (SON) shows the return of the gradient into the domain. Across seasons, the model maintains strong correspondence with observations (winter: RMSE = 0.08 mg/m³, r = 0.90; spring: RMSE = 0.15 mg/m³ , r = 0.94; summer: RMSE = 0.05 mg/m³, r = 0.83; Fall: RMSE = 0.05 mg/m³, r = 0.88).

The model also captures interannual chlorophyll variability, with temporal correlations exceeding 0.90 across most of the domain and reaching r > 0.95 in eutrophic waters north of 30°N (Fig. 8c). Anomaly RMSE values remain low throughout the domain (Fig. 8d), indicating that the model reproduces the dominant modes of interannual variability in biogeochemical surface properties.

https://doi.org/10.5194/egusphere-2026-1877
Preprint. Discussion started: 29 July 2026

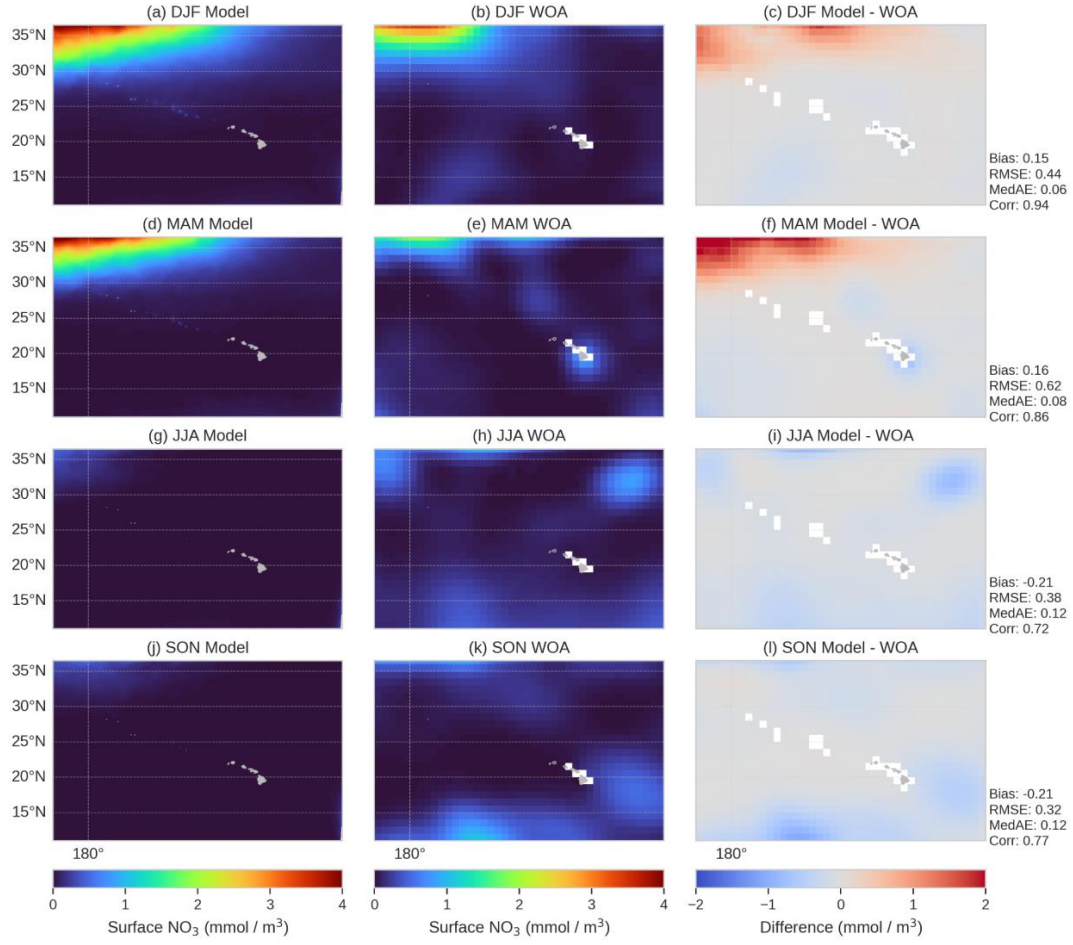

Figure 10. Seasonal comparison of surface nitrate concentrations between model and WOA climatology. HIC6k (left column), WOA observations (middle column), and their difference (Model - WOA, right column) for (a-c) Winter (DJF), (d-f) Spring (MAM), (g-i) Summer(JJA), and (j-l) Fall(SON). Difference panels show bias, RMSE, median absolute error (MedAE), and spatial correlation coefficient.

Surface nitrate distributions in the model demonstrate good agreement with World Ocean Atlas (WOA) climatology across all seasons (Fig. 10), successfully reproducing the characteristic contrasts between oligotrophic subtropical conditions and mesotrophic subpolar conditions that underlie the TZCF dynamics. The model maintains consistently low positive biases (0.15-0.16mmol/m³) during winter (DJF) and spring (MAM) with high spatial correlations (r=0.94 and 0.86, respectively), capturing the nutrient-depleted surface waters typical of the subtropical gyre and the north-south nutrient gradient associated with the TZCF. The model does not exhibit the patchiness evident in the objectively analyzed WOA fields, resulting in negative biases (-0.21 mmol/m³, for both) with RMSE values of 0.38 and 0.32 mg/m³, respectively. The WOA, however, includes data collected using a variety of methodologies of varying precision, and is most reliable for contrasts across the TZCF. Comparison with consistent high-precision measurements at station ALOHA show that persistent nanomolar NO_3 concentrations simulated by the model within the NPSG are consistent with those observed (see Section 3.3).

https://doi.org/10.5194/egusphere-2026-1877
Preprint. Discussion started: 29 July 2026

The model also successfully simulates low levels of observed phosphate (Fig. S3a) that has been identified as an important control on nitrogen fixation in the NPSG (Karl et al., 1997; Moutin et al., 2008; Watkins-Brandt et al., 2011). As discussed in the methods section, this result was sensitive to both the phosphate data used for the ocean boundary conditions and the degree of P-frugality afforded to phytoplankton populations.

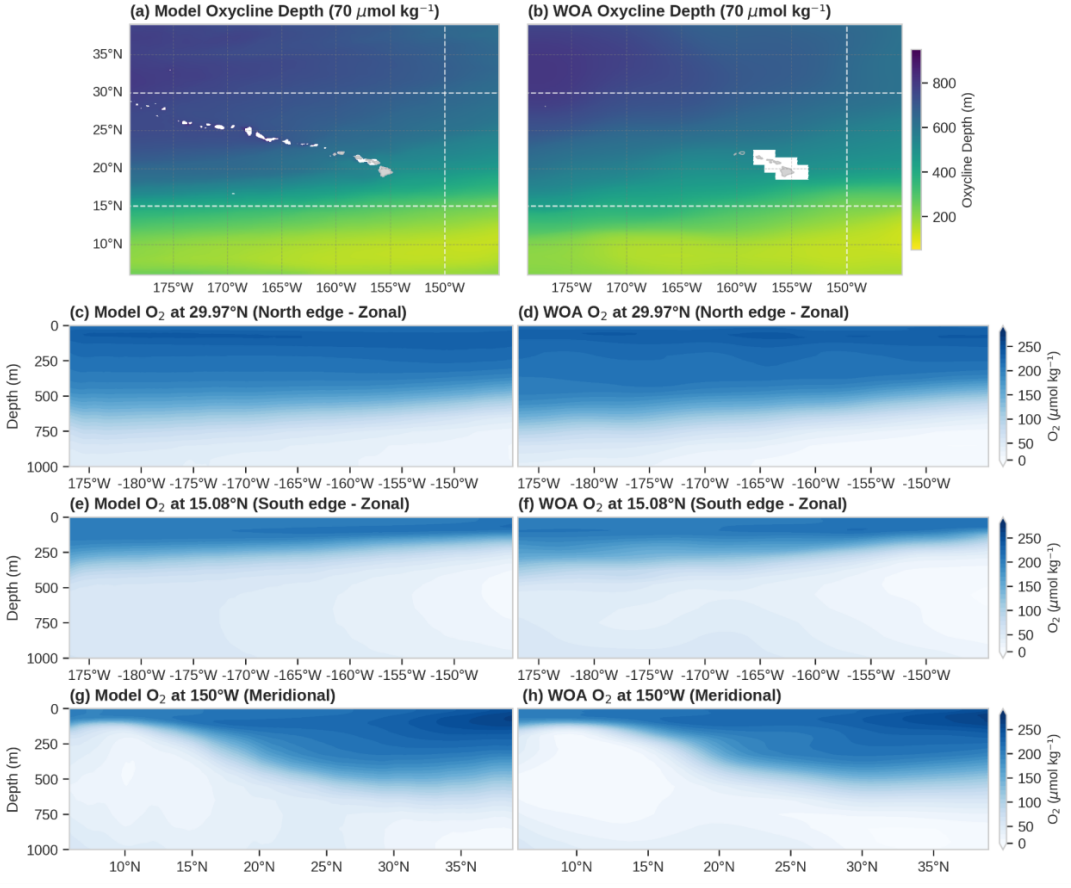

Figure 11. Comparison of oxycline depth and zonal oxygen sections between model and observations. (a-b) Spatial distribution of oxycline depth (depth of 70 µmol kg^{-1} oxygen isoline) from model and WOA climatology, showing the oxygen minimum zone structure. (c-f) Zonal sections of dissolved oxygen concentration in model and WOA observations along two latitudes: (c,d) 29.97°N, (d,e) 15.08°N, and meridional section along (g,h) 150°W. The oxycline shoals from >800 m in the subtropics to <200 m in the central North Pacific oxygen minimum zone.

The model resolves vertical and horizontal gradients in dissolved oxygen concentrations across the NPSG (Fig. 11). Oxycline depth, defined as the depth where oxygen concentration falls below 70 µmol kg^{-1} (approximately 1.5 ml L^{-1}, a threshold relevant to bigeye tuna fishery habitat compression; Prince and Goodyear 2006), exhibits strong equatorward shoaling in both the model (Fig. 11a) and World Ocean Atlas climatology (Fig. 11b), ranging from >800 m at 35°N to <100 m near 10-12°N. The model accurately reproduces this meridional oxycline structure with high spatial fidelity, capturing the characteristic shallow oxygen minimum zone (OMZ) in tropical waters and the deepening of well-oxygenated surface waters toward higher latitudes. The model reproduces localized oxycline

https://doi.org/10.5194/egusphere-2026-1877
Preprint. Discussion started: 29 July 2026

variations around the Hawaiian Islands (approximately 20°N, 160°W), where island wake effects and mesoscale circulation features modulate oxygen distributions.

Vertical cross-sections demonstrate the model's skill in resolving the three-dimensional structure of the oxygen field and its pronounced meridional gradient. A meridional transect at 150°W (Fig. 11g) reveals the "bowl" structure of the North Pacific Subtropical Gyre, with well-oxygenated surface waters (>200 μmol kg^{-1}) deepening from <200 m at the southern boundary to >400 m near 30°N before shoaling again toward the northern edge. The oxycline rises dramatically toward both gyre edges: oxygen-depleted waters (<70 μmol kg^{-1}) shoal from >800 m at 30°N to <200 m near 15°N, with the core OMZ (<45 μmol kg^{-1}) centered around 400-600 m depth in tropical waters. This steep meridional gradient in oxycline depth directly corresponds to the north-south limits of Hawaii-based longline fishing operations.

Zonal transects further illustrate regional oxygen variability. At 29.97°N (Fig. 11c), oxygen concentrations exceed 200 μmol kg^{-1} throughout the upper 400 m, characteristic of well-ventilated subtropical mode waters, with gradual depletion to 45-75 μmol kg^{-1} below 600 m depth. At 15.08°N (Fig. 11e), the transect captures the core OMZ region, where oxygen concentrations below 45 μmol kg^{-1} extend from approximately 200-800 m depth, with particularly intense depletion (15-30 μmol kg^{-1}) centered around 400-600 m. A prominent vertical feature in both transects near the Hawaiian Islands corresponds to enhanced vertical mixing that disrupts the stratified oxygen structure. This capability to resolve oxycline shoaling with its steep meridional gradient and realistic depth ranges and spatial patterns is crucial for bigeye tuna habitat modeling, as the species exhibits strong behavioral preferences for oxygen thresholds above 60-70 μmol kg^{-1} and is vertically constrained by oxycline depth.

Beyond the mean oxycline structure, we evaluated the model's ability to capture interannual variability in oxygen distributions by comparing temporal evolution of oxycline depth with the GOBAI-O_2 oxygen product (Fig. S4). Both the model (Fig. S4a) and GOBAI-O_2 (Fig. S4b) show the characteristic meridional gradient in oxycline depth from >600 m at 30-35°N to <200 m near 10-15°N throughout the 2004-2019 period. Interannual anomalies along 150°W (Fig. S4c-d) reveal limited temporal correlation between the model and GOBAI-O_2 (r=0.19, RMSE=38.9 m), with the model exhibiting greater local variability (1.83× GOBAI-O_2). At the domain-average scale, the two products show better agreement (r = 0.67, RMSE = 6.7 m; Fig. S4e), though the model does not reproduce the progressive shoaling trend evident in GOBAI-O_2 over 2004–2019.

3.3 The Oligotrophic Gyre Ecosystem

After establishing basin-scale physical and biogeochemical patterns, we examined the model's ability to resolve the characteristic features of the oligotrophic NPSG using observations from Station ALOHA. This long-term observational platform provides a critical benchmark for evaluating model performance in the open-ocean environment that dominates much of the subtropical North Pacific high seas region, and an additional assessment of the simulation’s capacity to capture temporal variability.

https://doi.org/10.5194/egusphere-2026-1877
Preprint. Discussion started: 29 July 2026

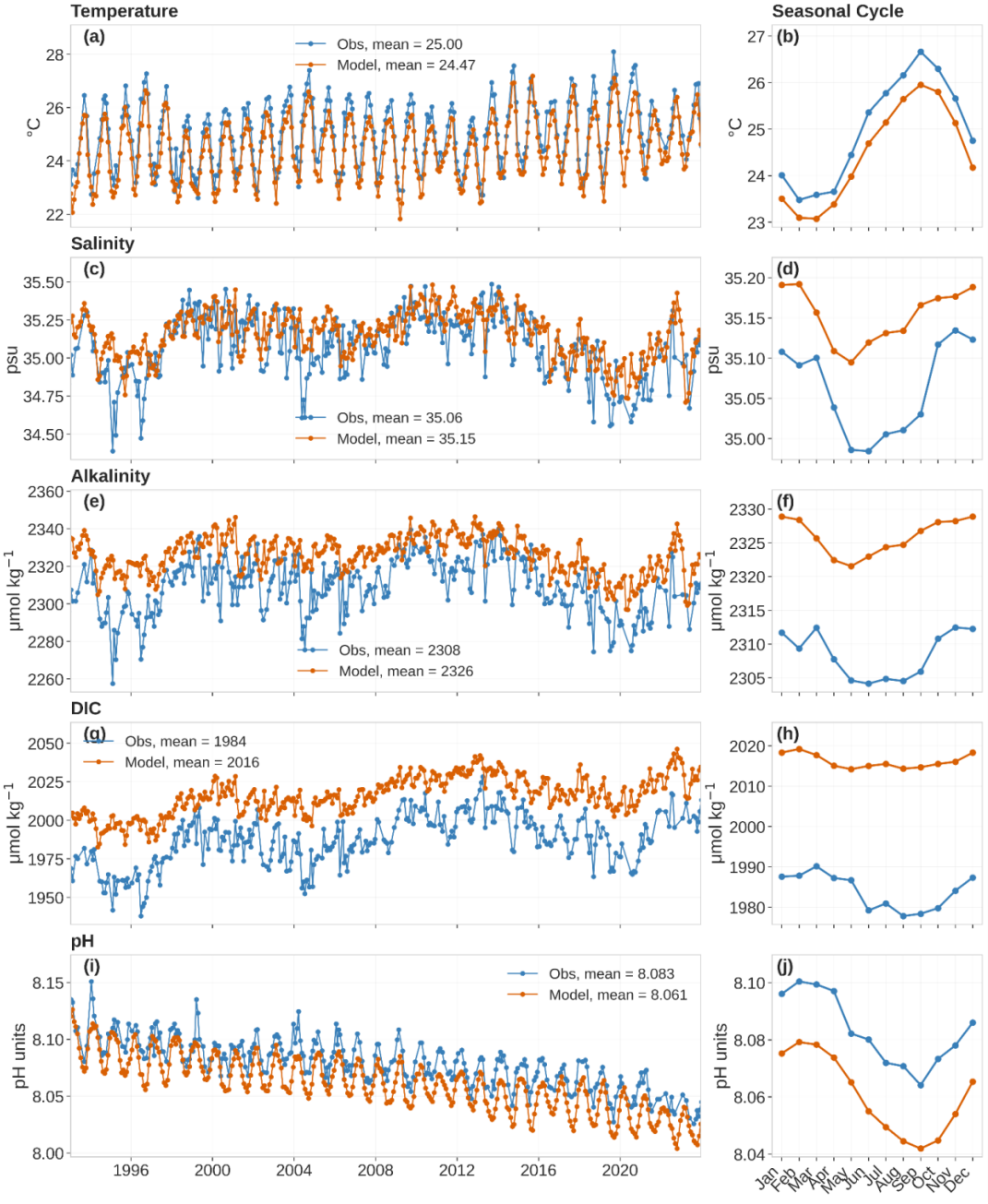

Figure 12. Time series and seasonal climatologies of near-surface ocean properties at Station ALOHA. Left column shows monthly time series from 1993-2023 for (top to bottom) temperature (°C), salinity (psu), dissolved inorganic carbon (DIC), and pH, comparing model output (orange) with Station ALOHA observations (blue). The right column shows corresponding seasonal climatologies averaged across all years.

https://doi.org/10.5194/egusphere-2026-1877
Preprint. Discussion started: 29 July 2026

At Station ALOHA, the model reproduces seasonal and interannual patterns in ocean surface parameters over the 1993-2023 period (Fig. 12), though with systematic biases in several variables.

Near-surface temperature showed strong agreement with observations. The model reproduced both the mean state (24.4°C modeled vs. 25.0°C observed) and the characteristic seasonal cycle, with warmer temperatures in summer-fall (July-October, ~26-27°C) and cooler temperatures in late winter-early spring (February-April, ~23-24°C). The model tracked interannual variability well throughout the time series, including warmer periods in the late 1990s, mid-2000s, and 2014-2020 (Fig. 12b).

Near-surface salinity (Fig. 12c-d) exhibited a consistent, modest positive bias throughout the record (35.15 psu modeled vs. 35.06 psu observed). The model captured the interannual trends, including the freshening period from 2010-2020, but showed reduced seasonal amplitude compared to observations, with the observed late winter-spring salinity minimum (~35.00 psu) overestimated by the model.

The carbonate system parameters showed moderate agreement but with small yet systematic biases partially attributable to the elevated model salinity. Near-surface alkalinity was overestimated by approximately 20 μmol kg^{-1} (2326 μmol kg^{-1} modeled vs. 2308 μmol kg^{-1} observed), dissolved inorganic carbon by 31 μmol kg^{-1} (2016 vs. 1984 μmol kg^{-1}), and pH was underestimated (8.061 vs. 8.083). Despite these biases, the model successfully tracked observed temporal trends from 1993-2023 and captured key seasonal patterns including summer alkalinity and pH minima and winter-spring maxima (Fig. 12e-j).

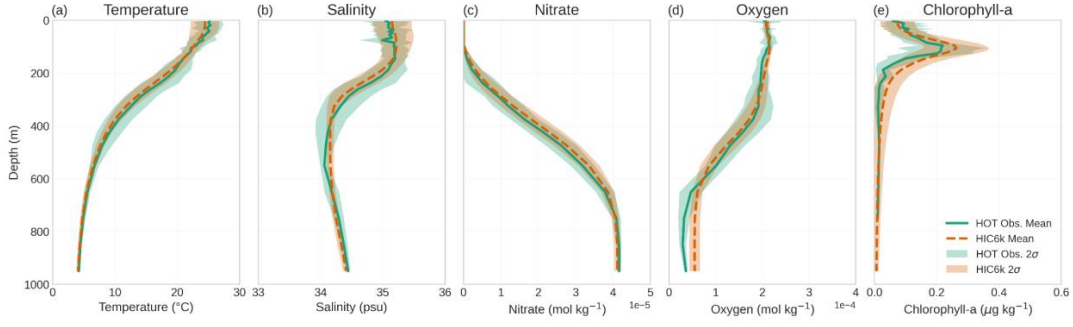

Figure 13. Vertical profiles of oceanographic and biogeochemical properties at Station ALOHA. Mean profiles (0-1000 m depth) of temperature (ºC), salinity (psu), nitrate (mol kg^{-1}), dissolved oxygen (mol kg^{-1}), and chlorophyll-a (***μ***mol kg^{-1}), comparing HOT observations (green line) and model output from HIC6k (dashed orange line), with 2σ uncertainty bounds (shaded region green and orange respectively).

Comparison of modeled vertical profiles with Hawai‘i Ocean Time-series (HOT) observations revealed good overall agreement in representing major biogeochemical features through the upper 1000 m (Fig. 13). Temperature and salinity profiles showed strong agreement with observations, with the model accurately capturing the thermocline structure and salinity maximum near 200 m depth. The model successfully represented nutrient distributions across all depths, including surface depletion (<5 μmol/kg), a sharp nutricline at 100-300 m, and deep water nitrate+nitrite concentrations (~40-45 μmol/kg below 600 m) consistent with observations. Oxygen profiles captured near-surface saturation values (~200 μmol/kg) and the oxygen minimum zone between 400-800 m depth, with both the depth and intensity falling within observational uncertainty. Chlorophyll profiles reproduce the DCM near 100-150 m depth (~0.3-0.4 mg/m^3), though the model maintains elevated chlorophyll concentrations below the DCM compared to the sharper decline observed at Station ALOHA (Fig. 13e).

https://doi.org/10.5194/egusphere-2026-1877
Preprint. Discussion started: 29 July 2026

Unlike most ocean regions, focused plankton ecosystem observations at station ALOHA make it possible to assess the model's representation of a broader set of plankton foodweb properties. The biological production and standing stocks of foodweb components show reasonable agreement with observational estimates (Table 1). Modeled phytoplankton carbon (1348 mg C m^{-2}) and primary production (298 mg C m^{-2} d^{-1}) aligned well with field observations (1320-1533 mg C m^{-2} and 180-220 mg C m^{-2} d^{-1}, respectively). Particle export flux at 200m (11.9 mg C m^{-2} d^{-1}) was approximately half the observed value (26 mg C m^{-2} d^{-1}), suggesting the model may underestimate carbon export efficiency. Other biological components including bacterial carbon, microzooplankton, and mesozooplankton showed similar patterns, with carbon stocks generally within observational ranges but some underestimation in heterotrophic production rates.

Quantity	Low Chlorophyll Biome		Hawaiian Ocean times Series		
	HIC6k (200m) mg C m^{-2}	COBALT (Stock et al., 2014)	HIC6km (200m) mg C m-2	COBALT (stock et al., 2014)	Observations
Phytoplankton carbon	890	1017 (149)	1348	876	"1533a, 1320b"
Primary production	311	289 (101)	298	190	"492 (118)c, 180-220d"
Bacterial carbon	467	730 (119)	740	619	750-1500e
Bacterial production	54.5	27 (11)	50.5	16	NA
Microzooplankton carbon	334	494 (69)	501	431	NA
Microzooplankton production	25.9	40 (18)	23.1	20	NA
Mesozooplankton carbon	453	533 (191)	681	269	236 (107)f
Mesozooplankton production	13.6	14.5 (12.0)	11.6	2.4	"27 (8.8)j, 11k"
Total zooplankton carbon	787		1181		
Particle export flux	14.1	19.2 (9.3)	11.9	8.5	26 (6)j

a Campbell et al. (1994), based on microscope counts and carbon conversion factors (ccfs).
b Dunne et al. (2005) based on integrated chl and C:chl ratios.
c Karl et al. (1996) as reported in Roman et al. (2002), mix on on-deck and in situ 12 h 14C incubations.
d Boyd et al. (2008), 24 h on-deck 14C integrations.
e Ducklow (1999) range reflects carbon conversion factors of 10–20 fg C cell1 for biomass and 1.5–3 kg C mol1 for leucine incorporation.
f Roman et al. (2002).
f* Roman et al. (2002) but with Hirst and Bunker (2003) update for mesozooplankton growth estimate.
g DuRand et al. (2001).
h Steinberg et al. (2001).
i Roman et al. (1995a).

Table 1. Comparison of carbon stocks and fluxes between model simulations and observations for the Hawaiian ocean time-series region. Model estimates from HIC6km (200 m integrated values) and COBALT (Stock et al., 2014) are compared with field observations from the Hawaiian Ocean Time-series (HOT) program.

3.4 Island Wakes

Island-ocean interactions in the Hawaiian archipelago generate complex mesoscale circulation features that influence both physical dynamics and biogeochemical distributions. The model's representation of these wake dynamics provides insight into its capability to resolve the physical mechanisms that drive ecosystem variability around Pacific islands.

https://doi.org/10.5194/egusphere-2026-1877
Preprint. Discussion started: 29 July 2026

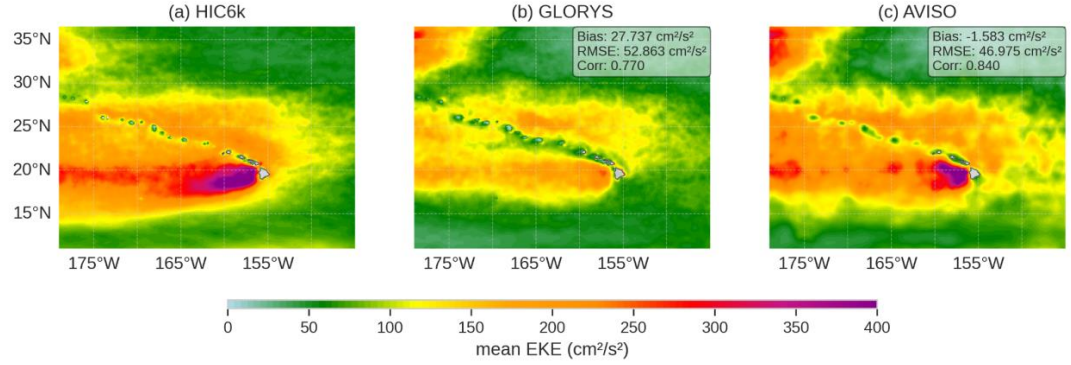

Figure 14. Comparison of mean eddy kinetic energy (EKE, cm^2/s^2) calculated from geostrophic currents for (a) HIC6k, (b) GLORYS12 reanalysis and (c) AVISO geostrophic velocities. All three EKE data sets were averaged for the time period 1993-2023.

Comparison of mean eddy kinetic energy (EKE) with AVISO altimetry and GLORYS12 reanalysis reveals that the model now accurately captures mesoscale variability in the Hawaiian lee region (Fig. 14). With the optimized current feedback parameter (α_{cfb}=0.2), the model shows close agreement with observational products. The model successfully reproduces both the spatial pattern and the magnitude of enhanced mesoscale activity in the downstream wake zones where island-generated eddies and flow disturbances are most prominent. The Hawaiian lee region shows elevated EKE relative to upstream waters and the surrounding oligotrophic gyre, with peak values exceeding 400 cm^2/s^2 concentrated around 20° N near the main Hawaiian Islands, consistent with altimetry observations.

https://doi.org/10.5194/egusphere-2026-1877
Preprint. Discussion started: 29 July 2026

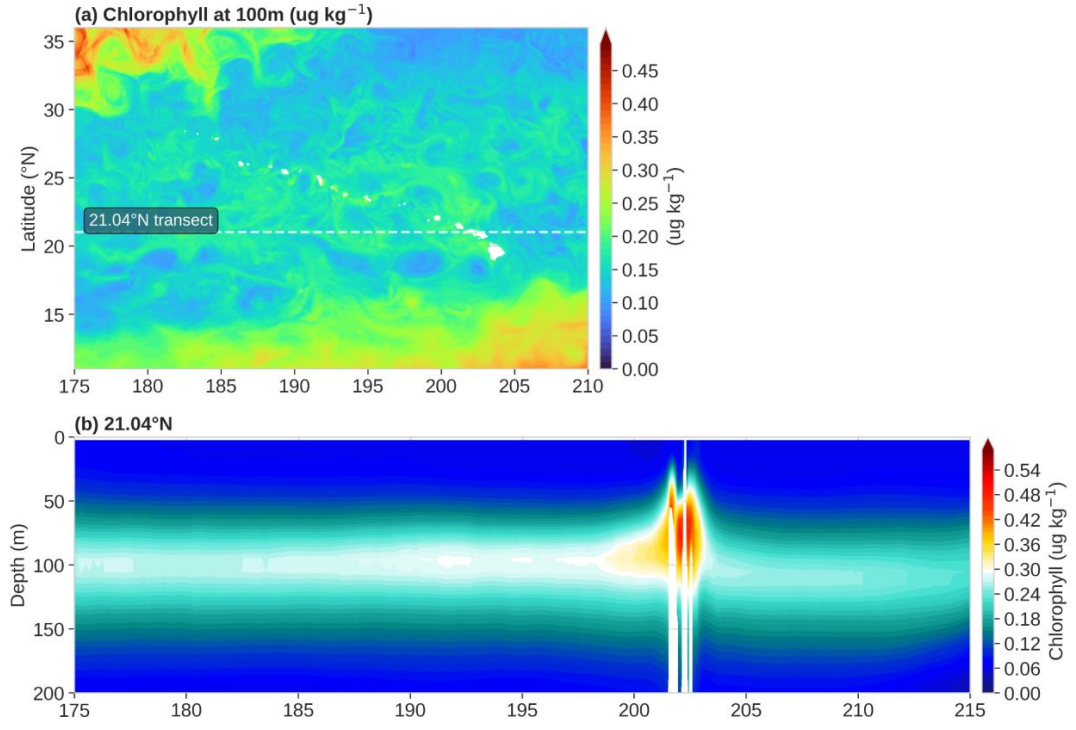

Figure 15. Chlorophyll-a distribution (a) at the deep chlorophyll maximum (DCM) and (b) along a 21.04°N vertical transect.

The biogeochemical consequences of island wake dynamics are evident in the spatial distribution of chlorophyll at 100m and its vertical structure (Fig. 15). Surface chlorophyll concentrations across the NPSG reveal the oligotrophic conditions characteristic of this region, with values typically below 0.20 µg kg⁻¹ throughout most of the domain (Fig. 15a).

The vertical transect along 21.04°N, which crosses the Hawaiian island chain, provides insight into the subsurface biogeochemical structure associated with island wake effects (Fig. 15b). Throughout most of the transect west of 200°E, chlorophyll concentrations remain low (<0.16 µg kg⁻¹) and exhibit typical oligotrophic vertical structure with a subsurface chlorophyll maximum between 50-100m depth. Near the island chain around 200-203°E, a distinct subsurface feature appears with elevated chlorophyll concentrations (up to 0.56 µg kg⁻¹) extending from approximately 50-150m depth.

3.5 Nearshore Temperature Variability

We evaluated model performance against in-situ measurements from 141 NCRMP monitoring locations distributed across Hawai‘i, Maui, O‘ahu, Kaua‘i, Moloka‘i, Lāna‘i, Ni‘ihau, Molokini, Lehua, French Frigate Shoals, Laysan, Lisianski, Pearl and Hermes Atoll, and Kure (Fig. 2). To illustrate the model's characteristic behavior and our analysis approach, we first examine a representative monitoring site off Maui Nui (20.95°N, 203.85°E; Fig. 16a) before presenting statistical comparisons across all 141 sites.

https://doi.org/10.5194/egusphere-2026-1877
Preprint. Discussion started: 29 July 2026

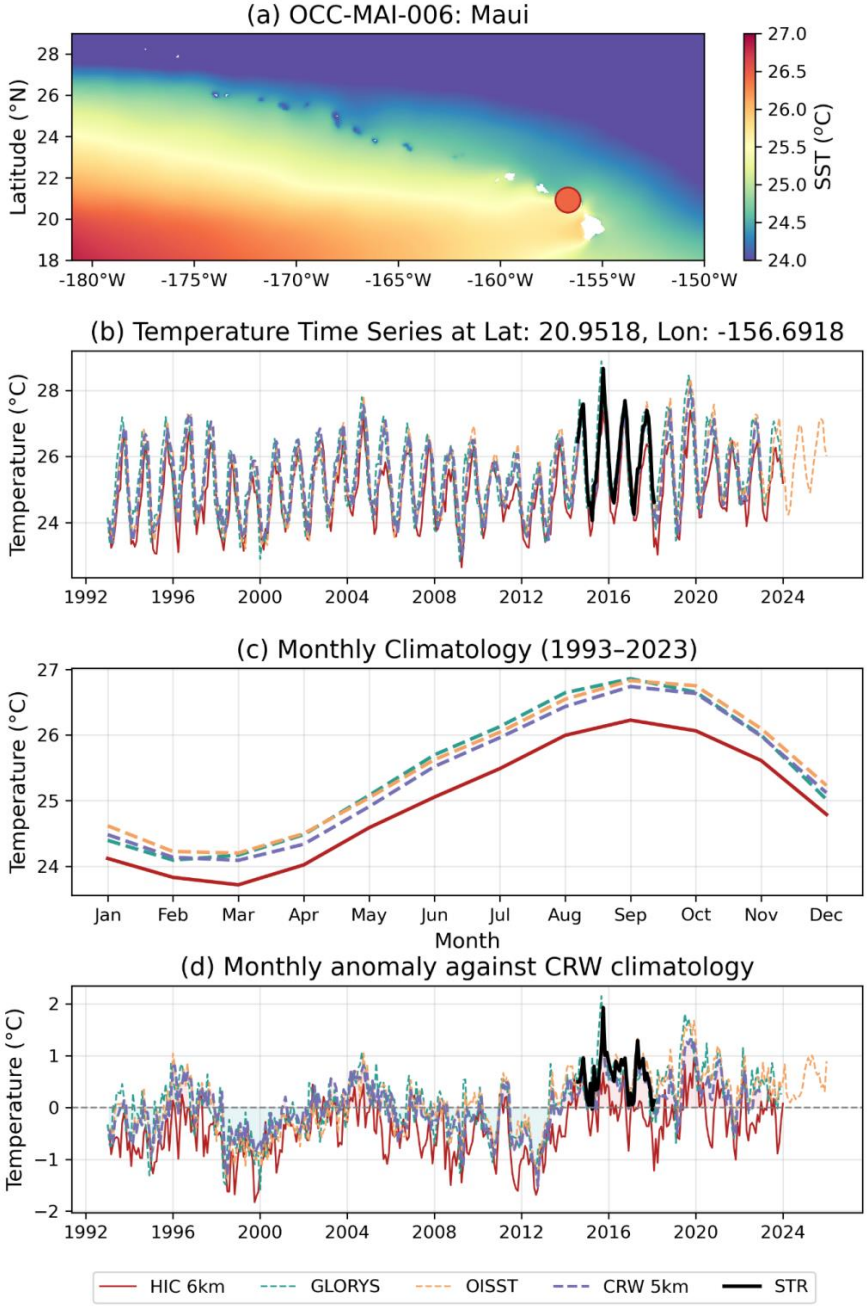

Figure 16. Sea surface temperature analysis at NCRMP monitoring location during the 2015 bleaching event. (a) Spatial map of mean SST (1993-2023) showing the Northwest and main Hawaiian Islands with a red circle indicating the analysis location in Maui Nui (20.95°N, 203.31°E). (b) Monthly SST time series (1992-2023) comparing model output (HIC 6km, dark red line) with GLORYS12 reanalysis (green dashed line), OISST

https://doi.org/10.5194/egusphere-2026-1877
Preprint. Discussion started: 29 July 2026

observations (orange dashed), CRW 5km (purple dashed line) and STR (black solid). (c) Monthly climatology (1993-2023) for HIC6k (dark red solid), GLORYS12 (green dashed), OISST (orange dashed) and CRW 5km (purple dashed). (d) Monthly temperature anomaly relative to CRW 5km climatology (1993-2023).

At this Maui site (Fig. 16), we compare the HIC6k model against the in-situ NCRMP monitoring site measurements, GLORYS12 reanalysis, OISST and the CRW 5km satellite products. The HIC6k model tracks the in-situ temperature variations through nearly three decades, capturing both the seasonal cycle and interannual variability (Fig. 16b). All products, including HIC6k, exhibit systematic differences relative to the in-situ observations. The model shows a consistent cold bias of approximately 0.5°C throughout the record (Fig. 16c), evident in the offset between the model's mean annual cycle (black line) and the STR climatology (red dashed line). However, when examining temperature anomalies relative to the CRW5km climatology (Fig. 16d), HIC6k successfully tracks the timing and magnitude of interannual temperature variations, including the prominent 2015 warming event that triggered widespread coral bleaching across Hawai‘i. This demonstrates that while the model has a systematic offset in absolute temperature, it accurately captures interannual variability.

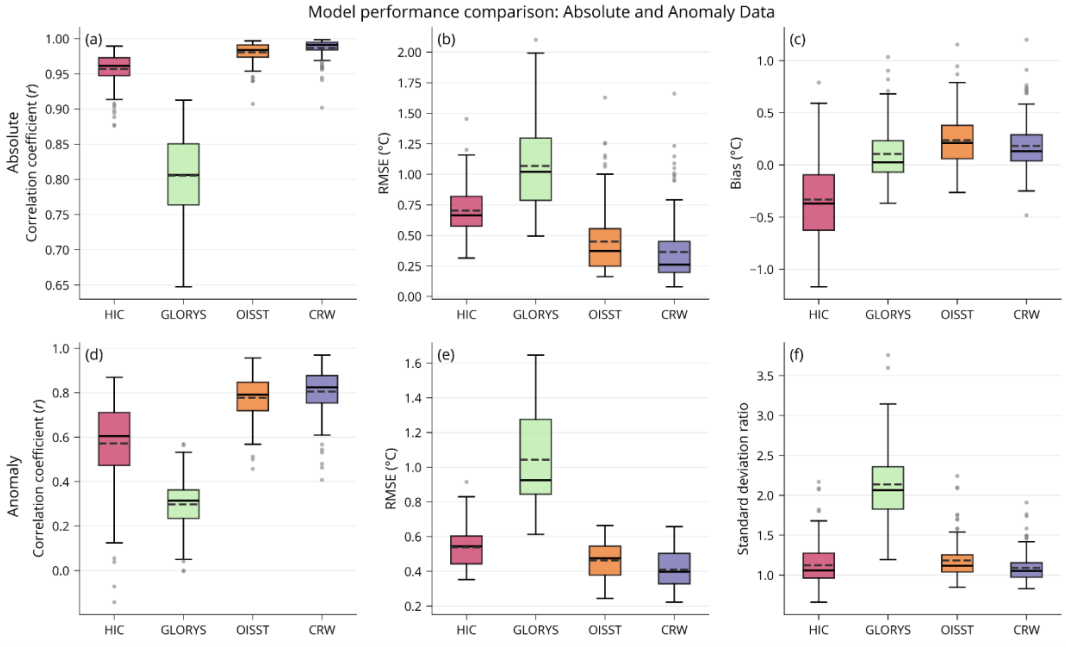

Figure 17. Statistical comparison of model, reanalysis and satellite products performance against in-situ STR observations across all 141 NCRMP monitoring locations. Box plots showing the distribution of correlation coefficient (r), root mean square error (RMSE), bias and standard deviation ratio for (top row) absolute values and (bottom row) deseasonalized anomalies. Products compared include: HIC 6km model (pink), GLORYS12 reanalysis (green), OISST satellite product (orange), and CRW 5km satellite product (purple). All metrics are calculated relative to in-situ STR measurements. Black solid lines represent the median, and black dashed lines represent the mean.

The strong temporal correlation despite systematic bias at this single Maui site is representative of model performance across the entire NCRMP monitoring network. Statistical comparisons of all four products against the 141 in-situ STR measurements show that the HIC6k model demonstrates strong skill in capturing nearshore

https://doi.org/10.5194/egusphere-2026-1877
Preprint. Discussion started: 29 July 2026

temperature variability, with a mean correlation coefficient of r = 0.96 (Fig. 17a). This performance exceeds the data-assimilative GLORYS12 global reanalysis (r = 0.80) and approaches the satellite products OISST (r = 0.98) and CRW 5km (r = 0.99). Model skill remains significant even when evaluating only interannual variability. After removing each product's mean seasonal climatology and comparing deseasonalized anomalies against in-situ STR observations (Fig. 17d), HIC6k maintains moderate correlations (mean r = 0.57), comparable to GLORYS12 (r = 0.53) and approaching satellite products OISST (r = 0.78) and CoralTemp (r = 0.81).

Root mean square errors (RMSE) are consistently low across all sites. The slightly higher RMSE for HIC6k, relative to GLORYS12 and OISST, is attributed to the model's systematic cold bias (-0.34°C) rather than a reduction in its ability to capture temporal variability. As demonstrated by the Maui example (Fig. 16), this cold bias is consistent across validation sites throughout the year. The standard deviation ratio (Fig. 17f) shows that all products capture comparable magnitudes of temporal variability relative to observations, with ratios near 1.0 indicating that the amplitude of modeled temperature fluctuations matches observed variability.

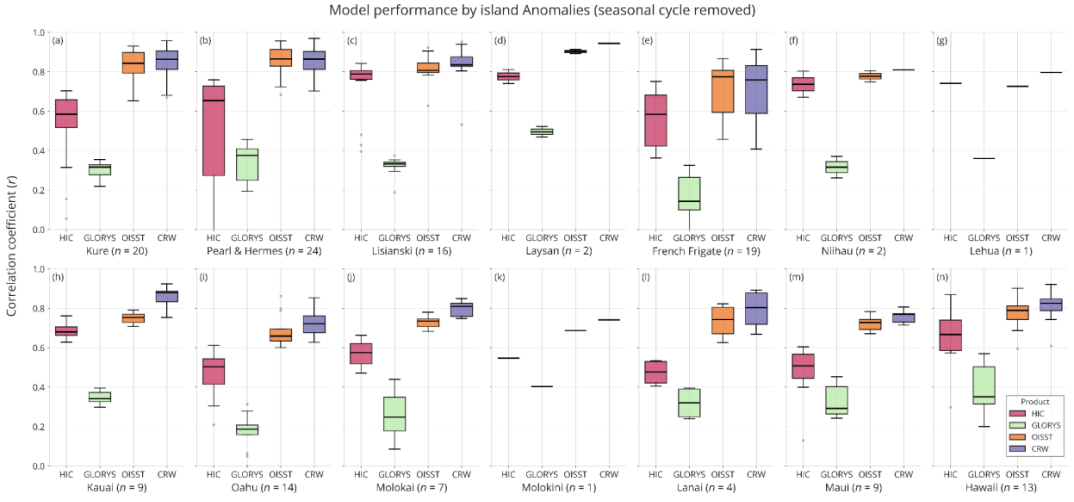

Figure 18. Correlation coefficients (r) of deseasonalized SST anomalies from four products compared against in situ STR observations across 141 NCRMP coral reef monitoring sites, grouped by island. Box plots show the distribution of r values for the HIC6k regional ocean model (pink), GLORYS12 reanalysis (green), OISST (orange), and CRW 5 km (purple) satellite products. All metrics are calculated relative to co-located STR measurements (Smith and Barkley, 2025; Perelman et al., 2024).

When monitoring sites are grouped by island, model performance varies across the Hawaiian archipelago (Fig. 18, Table 2). For deseasonalized anomalies, HIC6k correlation coefficients at the main Hawaiian Islands range from 0.47 (Maui) to 0.78 (Laysan Island), with performance comparable to or exceeding GLORYS12 (Table 2). Both satellite products (OISST and CRW 5km) consistently show higher correlations, as expected given their assimilation of observational data, with mean correlations ranging from 0.69-0.90 (OISST) and 0.71-0.94 (CRW 5km) across island groups.

https://doi.org/10.5194/egusphere-2026-1877
Preprint. Discussion started: 29 July 2026

Island	Avg N Months	Obs Mean (°C)	Obs Std (°C)	Bias (°C) (anomalies)			r (anomalies)			RMSE (°C) (anomalies)		
				HIC6k	GLORYS	OISST	HIC6k	GLORYS	OISST	HIC6k	GLORYS	OISST
French Frigate	50	25.21	1.65	-0.01	0.03	0.05	0.55	0.17	0.71	0.44	0.88	0.4
Hawaii	45	25.63	0.85	0.02	0.09	0.05	0.66	0.40	0.77	0.54	0.81	0.57
Kaua‘i	56	25.49	1.17	0.24	0.13	0.17	0.69	0.35	0.75	0.51	0.81	0.51
Kure	60	23.46	2.54	0.19	0.22	0.19	0.54	0.30	0.83	0.66	1.39	0.44
Lana‘i	52	25.59	0.92	-0.01	0.00	0.05	0.47	0.32	0.73	0.5	0.8	0.56
Laysan	49	24.96	1.97	0.09	-0.04	0.07	0.78	0.50	0.90	0.38	1.14	0.27
Lehua	35	25.18	0.93	-0.20	-0.40	-0.36	0.74	0.36	0.73	0.36	0.79	0.5
Lisianski	70	24.79	2.30	-0.02	0.01	0.00	0.73	0.32	0.82	0.43	1.12	0.37
Maui	43	25.32	0.94	0.02	0.10	0.13	0.47	0.34	0.72	0.6	0.83	0.59
Moloka‘i	49	25.26	0.94	0.13	0.20	0.21	0.57	0.26	0.73	0.49	0.82	0.55
Molokini	34	25.17	0.72	-0.50	-0.44	-0.41	0.55	0.40	0.69	0.65	0.82	0.56
Ni‘ihau	49	25.52	1.14	0.05	-0.04	-0.01	0.74	0.32	0.78	0.49	0.83	0.48
O‘ahu	43	25.63	1.18	0.27	0.36	0.35	0.47	0.17	0.69	0.51	0.89	0.5
Pearl & Hermes	67	23.67	2.40	0.01	0.15	0.09	0.50	0.34	0.86	0.63	1.35	0.43

Table 2. Statistical comparison of sea surface temperature anomaly (seasonal cycle removed) performance across Hawaiian Islands. Model (HIC6k), reanalysis (GLORYS), OISST observations and CRW 5km dataset performance metrics compared against STR observations for fourteen Hawaiian Islands: Hawaiian Islands: French Frigate Shoals, Hawai‘i, Kaua‘i, Kure Atoll, Lāna‘i, Laysan Island, Lehua, Lisianski, Maui, Moloka‘i, Molokini, Ni‘ihau, O‘ahu and Pearl and Hermes Atoll. Columns show the average number of months with data, mean temperature from STR dataset, standard deviation of STR temperatures, bias relative to observations, correlation coefficient (r) and RMSE for each product.

Root mean square errors for HIC6k range from 0.36°C (Lehua) to 0.69°C (Molokini) for deseasonalized anomalies (Table 2). The observed mean temperatures at monitoring sites show remarkable consistency across the main Hawaiian Islands (25.17-25.63°C), while the standard deviation of observations varies from 0.72°C (Molokini) to 2.54°C (Kure), reflecting differences in the strength of seasonal cycles and interannual variability at different locations, with the Northwestern Hawaiian Islands showing greater variability due to their higher latitude.

4. Discussion

Our objective is to develop and evaluate a regional ocean biogeochemical modeling system designed to support marine resource management in Pacific Island ecosystems. This requires a system that captures a range of scales, from basin-scale pelagic habitat dynamics to localized coastal thermal stress, sufficiently well. The HIC6k configuration demonstrates substantial skill across all three scales examined, though with varying levels of fidelity that provide clear targets for future refinement.

The HIC6k configuration occupies a unique niche in Pacific Islands ocean modeling. Global Earth System Models provide basin-to-global context but typically operate at 50-100km (Roberts et al., 2020; Tsujino et al., 2024) resolution, too coarse to resolve island wakes, mesoscale productivity features, or nearshore gradients. High-resolution coastal models can capture reef-scale processes but require prescribed boundary conditions and cannot simulate basin-scale climate modes. Regional configurations like the Hawaiian Islands ROMS system have demonstrated skill for coral reef thermal stress assessment (Perelman et al., 2024), have proven valuable but lack the domain size to capture large-scale forcing or the biogeochemical complexity of food web applications. As part of NOAA’s Changing Ecosystems and Fisheries Initiative (CEFI), regional MOM6-based regional configurations are being developed for multiple U.S. regions reflecting growing recognition that multi-scale regional systems are essential to translate climate projections into actionable resource management information. The HIC6k configuration

https://doi.org/10.5194/egusphere-2026-1877
Preprint. Discussion started: 29 July 2026

serves as CEFI's initial Pacific Islands regional model, extending this capability to the NPSG and enabling analysis of how basin-scale climate forcing propagates through island-modified mesoscale processes to influence both pelagic and coastal ecosystems.

4.1 Model Suitability for Fisheries Applications

The model's basin-scale performance establishes a robust foundation for pelagic habitat-driver applications. Sea surface temperature is reproduced with strong spatial fidelity ($r > 0.95$ across most of the domain; Fig. 3a), and the model accurately captures seasonal TZCF migration in both temperature (18°C isotherm: $r = 0.97$, mean latitude varying ~10° between winter and summer; Fig. S2) and chlorophyll (0.2 mg/m³ transition; Fig. 9). Interannual variability is similarly well resolved, with temperature correlations exceeding 0.95 and chlorophyll skill ranging from 0.90 to 0.95, particularly north of 30°N (Fig. 8a,c). Together, these results demonstrate the model's capability to resolve the key oceanographic conditions that constrain pelagic habitat.

The TZCF, which migrates seasonally across approximately 1000 km from its southern winter position near 30-35°N to its northern summer extent around 40-45°N (Polovina et al., 2001, 2017; Bograd et al., 2004), represents a critical ecosystem boundary where loggerhead turtles, albacore tuna, and other apex predators concentrate during their migrations (Polovina et al., 2001; Kobayashi et al., 2008). Our model's capture of the TZCF's position (Fig. S2), its underlying seasonal variations in mixed layer depth and associated vertical mixing (Fig. 6), and horizontal transport of nutrients from higher latitudes (Fig. 10) indicates it can support habitat suitability modeling and projections of climate-driven distributional shifts for commercially important species.

The model's representation of oxygen distributions holds particular relevance for Pacific longline fisheries. The accurate simulation of equatorward oxycline shoaling from >800 m at 35°N to <100 m near 10-12°N for the 70 µmol kg^{-1} threshold, directly addresses habitat compression concerns for bigeye tuna (*Thunnus obesus*), the dominant target species in Hawaii-based longline fisheries. Bigeye tuna exhibit strong behavioral responses to dissolved oxygen thresholds around 60-70 µmol kg^{-1} (Prince and Goodyear 2006; Stramma et al., 2012), and observations of ~1.5 ml L^{-1} (approximately 67 µmol kg^{-1}) tolerance limits align closely with our chosen threshold. For longline fisheries management, however, a more operationally relevant consideration is where the 90 µmol kg^{-1} isopleth shoals above hook depth (~400m), as this boundary is hypothesized to define the geographic extent of fishable habitat and effectively excludes the southeastern portion of the model domain from productive fishing grounds. The model's capacity to resolve this mean-state oxygen structure provides a platform for assessing how projected ocean deoxygenation under climate change may compress vertical habitat and alter catch distributions (Stramma et al., 2012), information critical for ecosystem-based fisheries management. Nevertheless, characterizing the temporal variability of this boundary remains an important target for improvement, and we note that current observational products such as GOBAI-O_2 may themselves have limited capacity to resolve interannual variability in oxycline position, which complicates validation and underscores the need for sustained subsurface oxygen monitoring in the region (see Section 4.3).

At intermediate scales, the model resolves island wake effects and their biogeochemical consequences, capturing fundamental patterns such as the "island mass effect" (Doty & Oguri, 1956), whereby island-induced physical processes elevate local productivity above surrounding oligotrophic background levels. Our simulation of subsurface chlorophyll enhancement near the island chain (up to 0.56 µg kg^{-1}, 3-4x the surrounding oligotrophic background of ~0.08-0.16 µg kg^{-1}; Fig. 15b), coupled with realistic mesoscale variability patterns (Fig. 14), demonstrates the model's ability to resolve physical-biogeochemical interactions at island scales relevant to understanding ecosystem function and productivity in Pacific island systems.

The model's performance at Station ALOHA further demonstrates its capability to capture the fundamental characteristics of the oligotrophic subtropical gyre, including surface property variability across seasonal to decadal

https://doi.org/10.5194/egusphere-2026-1877
Preprint. Discussion started: 29 July 2026

timescales (Fig. 12), realistic vertical structure in temperature, salinity, nutrients, and oxygen through the upper 1000 m, and key features including the DCM and oxygen minimum zone (Fig. 13). Integrated biological metrics show reasonable agreement with observations, with modeled carbon stocks and primary production falling within observed ranges, though underestimation of export flux remains a target for future model refinement (Table 1; see Section 4.3).

At nearshore scales, the model's capacity to reproduce local temperature variations observed at coral reef monitoring sites demonstrates a critical capability for bridging basin-scale climate forcing to reef-scale impacts. The demonstrated skill across the spatially distributed NCRMP monitoring network (mean r = 0.96 across 141 sites; Fig. 17a), spanning from the main Hawaiian Islands to the Northwestern Hawaiian Islands, provides confidence that the model can support assessments of thermal habitat across the broader Pacific Islands domain, enabling evaluation of how climate variability and change propagate from open-ocean to coastal ecosystem scales. While the model exhibits a systematic cold bias (mean of -0.34°C; Fig. 17c), this offset does not diminish its skill in resolving the temporal structure of thermal variability.

The magnitude of this bias remains within the range acceptable for coral reef thermal stress applications, where the model's ability to capture the timing and relative magnitude of warming events is more critical than absolute temperature accuracy (Liu et al., 2014). NOAA's Coral Reef Watch operational monitoring system has established degree heating weeks (DHW) as the standard metric for bleaching risk assessment, with Alert Level 1 (4°C-weeks DHW) indicating bleaching risk and Alert Level 2 (8°C-weeks DHW) indicating widespread bleaching with mortality (Liu et al., 2017, 2018). DHW calculations accumulate thermal stress by summing positive temperature anomalies (relative to climatological maximums) over the preceding 12 weeks (84 days), making them sensitive to both the magnitude and duration of warming events. Because DHW depends on anomalies relative to climatological baselines rather than absolute temperatures, the model's systematic bias can be readily corrected through bias adjustment in post-processing. The model's temporal fidelity in capturing synoptic-to-intraseasonal variability (2-90 day timescales), modestly outperforming GLORYS12 reanalysis (mean r = 0.60 vs 0.57 for deseasonalized anomalies; Fig. 17d), provides the short-duration warm event detection critical for accurately accumulating heat stress over the 12-week DHW window. Moreover, the model's three-dimensional temperature structure offers a significant advantage over surface-only satellite products like Coral Reef Watch, as subsurface temperatures can differ substantially from sea surface temperature in stratified conditions and provide better predictors of coral thermal stress across much of the Pacific Islands region (Venegas et al., 2019).

4.2 Choices Critical for Model Performance

Several technical choices proved critical for model performance across scales, revealing sensitivities that provide guidance for future ocean modeling efforts. The initial underestimation of eddy kinetic energy relative to AVISO altimetry and GLORYS12 reanalysis (Fig. S1) revealed systematic limitations with direct implications for nutrient supply mechanisms. This bias stemmed from the surface wind stress formulation: since we use reanalysis winds that already incorporate current feedbacks, the relative wind formulation in MOM6 introduces double-counting that excessively damps mesoscale features (Renault et al., 2016, 2019). Implementation of the Renault et al. (2019) correction factor (α_{cfb}) substantially improved EKE representation, bringing model values into close agreement with AVISO and exceeding GLORYS12 (Fig. 14), demonstrating that careful attention to atmosphere-ocean coupling formulations is essential for resolving mesoscale eddy fields that drive productivity in oligotrophic gyres.

Biogeochemical boundary conditions, particularly for phosphate, emerged as a critical control on nitrogen fixation and thus nitrogen availability in the oligotrophic NPSG. The model successfully simulates the persistently low phosphate concentrations (<0.05 μmol kg^{-1}) observed in the subtropical gyre (Fig. S3a), which previous work has identified as an important control on diazotroph populations and nitrogen fixation rates (Karl et al., 2001; Martiny et

https://doi.org/10.5194/egusphere-2026-1877
Preprint. Discussion started: 29 July 2026

al., 2019). This result proved sensitive to both the phosphate data used for ocean boundary conditions and the degree of phosphorus frugality (essentially the flexibility of cellular P:C stoichiometry under P-limited conditions) afforded to phytoplankton populations in the COBALT biogeochemical model. Initial configurations using World Ocean Atlas phosphate fields, which include substantial numbers of lower-precision measurements incapable of accurately resolving nanomolar concentrations (Martiny et al., 2019), combined with a more aggressive "line of frugality" from Galbraith and Martiny (2015), led to considerable excess phosphate (Fig. S3b). Switching to higher-precision phosphate measurements for boundary conditions (GLODAP) and adopting a more conservative stoichiometric flexibility parameterization brought model phosphate into agreement with Station ALOHA observations. This sensitivity underscores the importance of high-quality nutrient boundary conditions for oligotrophic regions where nanomolar concentrations control ecosystem structure.

Accurate representation of light penetration proved essential for capturing the DCM and subsurface primary production characteristic of the oligotrophic NPSG. The exceptionally clear waters at Station ALOHA, with blue-green light penetration among the deepest observed in the global ocean (Morel et al., 1988), required calibration of the clear-water attenuation coefficient (k_{sw} = 0.018 m^{-1}) below the default Manizza et al. (2005) parameterization, a value consistent with the most penetrating wavelengths in clear, case I waters and validated against long-term HOT program observations. This adjustment, consistent with Friedrich et al., (2024), highlights a broader challenge in biogeochemical modeling, where default parameterizations are often tuned to global or basin-scale averages that may not capture the extreme optical clarity of subtropical gyres. The deep light penetration in these systems supports photosynthesis to greater depths, influencing the vertical distribution of primary production and the depth of the CDM (Fig. 7 & 13). Importantly, described in Section 2.2.1, because the Manizza scheme allows chlorophyll-dependent attenuation to dominate in productive waters, this calibration primarily affects oligotrophic regions while having minimal impact on island wake zones or coastal areas where elevated productivity naturally increases attenuation. This selectivity makes the adjustment appropriate for a regional domain spanning oligotrophic to mesotrophic conditions.

The model's modest systematic salinity biases, and their resulting effect on carbonate chemistry at Station ALOHA illustrate how errors in atmospheric forcing propagate through coupled biogeochemical systems. The modest positive salinity bias at Station ALOHA (+0.09 psu; Fig. 12c-d) accounts for approximately 35-40% of the alkalinity overestimation and 20-25% of the DIC overestimation. The tight coupling between seasonal cycles in salinity, alkalinity, and DIC suggests that biases in freshwater flux representation propagate systematically through the carbonate system. Recent high-resolution modeling studies around Hawai‘i have similarly encountered surface property biases linked to atmospheric forcing quality (Friedrich et al., 2021). Despite these systematic offsets in absolute values, the small magnitude of the biases and the model's accurate representation of temporal patterns (Fig. 12) suggest that the model correctly captures the balance between physical and biogeochemical processes. For applications requiring precise pH or carbonate chemistry thresholds, bias correction using long-term observational records like Station ALOHA provides a clear path forward, while the model's pattern fidelity supports studies of relative changes and variability. This underscores the importance of accurate surface forcing, particularly precipitation and evaporation fields, for biogeochemical applications where small perturbations in physical properties can amplify through coupled processes (e.g., implications for ocean acidification projections or coral aragonite saturation).

4.3 Targets for Future Development

Several enhancements could expand the HIC6k system's capabilities and address current limitations revealed through our evaluation. These improvements fall broadly into two categories: enhancements to boundary conditions and external forcing, and refinements to interannual biological process representation. Together, they would advance the model toward more skillful simulation of NPSG ecosystem dynamics across the range of climate impact and fisheries applications for which the system is designed.

https://doi.org/10.5194/egusphere-2026-1877
Preprint. Discussion started: 29 July 2026

Implementation of full time-varying biogeochemical boundary conditions through nesting within a data-assimilative global model represents a high-priority enhancement. Despite accurate reproduction of mean oxycline structure (Fig. 11), the model exhibits greater interannual variability in oxycline depth at 150°W compared to GOBAI-O_2 (1.83× GOBAI-O_2; Fig. S4c-d). This difference likely reflects the smoothing of real interannual signals in the ML-based GOBAI-O_2 product rather than a model deficiency. The more pressing limitation is the simulations's inability to reproduce the subtle shoaling trend in oxycline depth over 2004-2019 evident in GOBAI-O_2, which likely reflects the limitations of climalogical boundary conditions in transmitting long-term changes in lateral oxygen transport or progressive shifts in biological oxygen demand.

Similar limitations are apparent in the simulation's representation of phosphate variability. Long-term HOT program observations at station ALOHA reveal substantial subdecadal oscillations in surface phosphate concentrations (from < 60 nmol kg^{-1} to > 70 nmol kg^{-1}) over the past three decades (Karl et al., 2017) that this configuration does not resolve (Fig. S3). Letelier et al. (2019) found a link between these oscillations and the Pacific Decadal Oscillation (PDO) phase, suggesting the PDO affects upper-ocean stratification at Station ALOHA. When the PDO enhances stratification, the resulting decrease in input from below causes phosphate concentrations to drop. Compounding this, episodic iron inputs stimulate biological uptake, further depleting the available phosphate in the surface layer (Letelier et al., 2019). Reproducing these climate-driven oscillations would require two advances beyond the current configuration: time-varying biogeochemical boundary conditions to capture PDO-driven changes in large-scale circulation and subsurface nutrient supply at the lateral boundaries, and explicit representation of the iron cycle to capture the biological mechanism by which aeolian iron deposition modulates diazotroph activity and PO_4 drawdown. Although this simulation already incorporates time-varying atmospheric boundary conditions, these alone are insufficient to resolve the nutrient stoichiometry changes that emerge from the coupled ocean-atmosphere-ecosystem response. PDO-driven nutrient variability is largely mediated through changes in large-scale ocean circulation and ventilation rather than atmospheric forcing alone (Stramma et al., 2020; Duteil et al., 2018), requiring these signals to propagate through time-varying oceanic boundary conditions that the current climatological configuration cannot provide. Time-varying biogeochemical boundary conditions would more broadly improve the model's ability to respond to decadal trends and constrain lateral fluxes, potentially reducing physical biases such as the salinity offset observed at Station ALOHA (Fig. 12) and improving interannual skill across multiple biogeochemical tracers.

While this configuration reproduces the DCM depth and magnitude at Station ALOHA, it maintains elevated chlorophyll concentrations below the DCM compared to the sharper decline observed (Fig. 13), a pattern also evident in basin-wide oligotrophic region profiles (Fig. 7). Potential mechanisms underlying this bias include inadequate top-down control from light-dependent grazing by microzooplankton, which in nature suppresses phytoplankton biomass near the surface while permitting accumulation at depth (Moeller et al., 2019), and potential limitations in the representation of self-shading below the chlorophyll maximum, where the dense DCM layer can strongly attenuate light for cells immediately below the peak (Morel & Maritorena, 2001). Addressing these would help sharpen the subsurface chlorophyll tail and have downstream benefits for carbon export efficiency and food web dynamics (Burd et al., 2024). Beyond phytoplankton dynamics, zooplankton in the NPSG are also known to perform extensive diel vertical migration (DVM), feeding in surface waters at night and descending to mesopelagic depths during the day, actively transporting carbon well below the euphotic zone via respiration, excretion, and fecal pellet production at depth (Al-Mutairi & Landry, 2001; Steinberg & Landry, 2017). Regional modeling suggests DVM-mediated active transport represents a secondary but non-negligible component of biological pump sequestration relative to gravitational settling (Poupon et al., in press). Incorporating zooplankton DVM into the model configuration would improve the representation of active carbon flux to the mesopelagic, though this process is unlikely to resolve the broadening of the chlorophyll profile below the DCM peak, which is more plausibly governed by phytoplankton dynamics and light attenuation. Nonetheless, this inclusion would enhance the model's utility for carbon export representation, and fisheries and ecosystem-based management applications.

https://doi.org/10.5194/egusphere-2026-1877
Preprint. Discussion started: 29 July 2026

Finally, the current configuration's treatment of streams as dissipating in wave-breaking zones remains appropriate for the open-ocean and reef-scale applications demonstrated here, with finer nearshore resolution representing a natural avenue for future development. Riverine freshwater inputs and submarine groundwater discharge operate at scales of tens to hundreds of meters yet deliver significant nutrient fluxes to Hawaiian coastal ecosystems (De Carlo et al., 2007; Peterson et al., 2009), and incorporating these processes alongside enhanced coastal resolution could support nearshore water quality assessment and land-sea interactions studies particularly relevant for high island systems. Given the importance of oxycline depth for bigeye tuna habitat, the projected expansion of oxygen minimum zones under climate change (Stramma et al., 2012), and the sensitivity of NPSG nitrogen cycling to climate-driven nutrient oscillations, improving interannual biogeochemical skill across oxygen, nutrients, and ecosystem structure represents the central target for the next generation of HIC6k development.

5. Conclusions

The HIC6k regional ocean biogeochemical model demonstrates the requisite skill to support fisheries and marine resource management applications across the diverse scales relevant to Pacific Island ecosystems. Basin-scale fidelity in temperature, nutrients, and oxygen provides a robust foundation for pelagic habitat modeling. Resolution of island wake effects, despite quantitative limitations in eddy intensity, captures the essential mechanisms by which islands modify oligotrophic ecosystems. Nearshore temperature skill enables coastal applications including coral reef thermal stress assessment. The systematic biases identified in salinity propagation through carbonate chemistry and EKE underestimation, prove clear targets for future refinement while not substantially undermining current utility.

This configuration represents a significant step toward integrated ecosystem modeling for Pacific Islands marine resource management, bridging the gap between global climate projections and local-scale ecosystem impacts. The model provides a platform for assessing how basin-scale climate variability and change propagate through island-modified processes to influence the pelagic and coastal ecosystems that support Pacific Island communities, economies, and food security.

Code availability

All MOM6 source code and other NOAA-GFDL model components used in this study are archived together at https://doi.org/10.5281/zenodo.19478039 (Negrete García et al., 2026a). Source code was originally sourced from the relevant upstream GitHub repositories, including MOM6 (https://github.com/mom-ocean/MOM6, Modular Ocean Model, 2026); https://github.com/NOAA-GFDL/MOM6, NOAA-GFDL, 2026a), and the CEFI regional configuration (https://github.com/NOAA-GFDL/CEFI-regional-MOM6, NOAA-GFDL, 2026b). Alkalinity and DIC were estimated using the ESPER algorithm of Carter et al. (2021), archived at https://doi.org/10.5281/zenodo.5512697, (Carter, 2021).

Data availability

The datasets used to construct model forcing, with corresponding access information, are as follows: the GLORYS12 reanalysis (https://doi.org/10.48670/moi-00021, Lellouche et al., 2021); the OSU TPXO9 Tide Model (https://www.tpxo.net/home, Egbert and Erofeeva, 2002); the World Ocean Atlas (2018) (https://www.ncei.noaa.gov/archive/accession/NCEI-WOA18); ERA5 Reanalysis (https://doi.org/10.24381/cds.adbb2d47, Hersbach et al., 2023); atmospheric CO_2 concentrations from Meinshausen

https://doi.org/10.5194/egusphere-2026-1877
Preprint. Discussion started: 29 July 2026

et al. 2016 (https://doi.org/10.22033/ESGF/input4MIPs.1118); and the GFDL ESM4.1 model output prepared for the CMIP6 historical experiment (https://doi.org/10.22033/ESGF/CMIP6.8597, Krasting et al., 2018).

All analyzed model output and the analysis codes used to produce this work are archived at https://doi.org/10.5281/zenodo.19486919 (Negrete García et al., 2026c). Model parameter files, forcing files, and initial condition files are separately archived at https://doi.org/10.5281/zenodo.19485393 (Negrete García et al., 2026b). Datasets used for model validation and comparison with their corresponding access URLs or DOIs, are listed below: OISSTv2.1 (https://www.ncei.noaa.gov/products/optimum-interpolation-sst, Huang et al., 2021); the GLORYS12 reanalysis (https://doi.org/10.48670/moi-00021, Lellouche et al., 2021); global ocean mixed layer depth climatology from de Boyer Montégut (https://doi.org/10.17882/98226, de Boyer Montégut, 2024); the World Ocean Atlas 2023 Nitrate, Phosphate, and Oxygen Output (https://doi.org/10.25923/39qw-7j08, Garcia et al., 2023a; https://doi.org/10.25923/rb67-ns53, Garcia et al., 2023b); the Hawaii Ocean Time-series surface CO2 system data product (https://hahana.soest.hawaii.edu/hot/hotco2/hotco2.html, Dore et al., 2009); ARGO float data (http://doi.org/10.17882/42182; Argo, 2026); AVISO altimetry data (https://doi.org/10.48670/moi-00148; AVISO, 2023); STR temperature observations across NCRMP monitoring stations (https://www.ncei.noaa.gov/erddap/tabledap/CRCP_Subsurface_Temp_Hawaii.html; NCEI accession #s 0162219, 0162216, 0210383, 0300489); NOAA Coral Reef Watch 5km temperature Product (https://coralreefwatch.noaa.gov/product/5km/index.php; NOAA Coral Reef Watch, version 3.1; Liu et al., 2014; Skirving et al., 2020). GOBAI-O2 data for supplement from (https://doi.org/10.5194/essd-15-4481-2023; Sharp et al. 2023).

Author contributions

ACR, CAS, and JYL contributed the source code for regional MOM6, COBALT, and/or other model framework components. YCT, CAS and ACR contributed to the workflow for easier generation of model input files. GNG and DM generated and assembled the model input files. GNG, CAS, ACR, and DM evaluated and interpreted the model results. GNG, DM and CAS wrote the initial draft of the manuscript. All coauthors contributed to discussions throughout the model development and evaluation and reviewed and approved the final manuscript.

Competing interests

At least one of the (co-)authors serves as topic editor for the special issue to which this paper belongs.

Acknowledgments

This work was conducted as part of NOAA's Changing Ecosystems and Fisheries Initiative. We thank Xiao Liu and Kyung-Min Noh for their helpful comments during the NOAA-GFDL internal review process.

Financial support

Co-authors Brian Powell and Tobias Friedrich were supported by NOAA MAPP (grant #NA24OARX431C0048).

References

https://doi.org/10.5194/egusphere-2026-1877
Preprint. Discussion started: 29 July 2026

Adcroft, A. and Campin, J.-M.: Rescaled height coordinates for accurate representation of free-surface flows in ocean circulation models, Ocean Model., 7, 269–284, https://doi.org/10.1016/j.ocemod.2003.09.003, 2004.

Adcroft, A., Anderson, W., Balaji, V., Blanton, C., Bushuk, M., Dufour, C. O., Dunne, J. P., Griffies, S. M., Hallberg, R. W., Harrison, M. J., Held, I., Jansen, M. F., John, J., Krasting, J. P., Langenhorst, A., Legg, S., Liang, Z., McHugh, C., Radhakrishnan, A., Reichl, B. G., Rosati, T., Samuels, B. L., Shao, A., Stouffer, R., Winton, M., Wittenberg, A. T., Xiang, B., Zadeh, N., and Zhang, R.: The GFDL Global Ocean and Sea Ice Model OM4.0: model description and simulation features, J. Adv. Model. Earth Sy., 11, 3167–3211, https://doi.org/10.1029/2019MS001726, 2019.

Al-Mutairi, H. and Landry, M. R.: Active export of carbon and nitrogen at Station ALOHA by diel migrant zooplankton, Deep-Sea Res. Pt. II, 48, 2083–2103, https://doi.org/10.1016/S0967-0645(00)00174-0, 2001.

Archibald, K. M., Siegel, D. A., and Doney, S. C.: Modeling the impact of zooplankton diel vertical migration on the carbon export flux of the biological pump, Global Biogeochem. Cy., 33, 181–199, https://doi.org/10.1029/2018GB005983, 2019.

Argo (2026). Argo float data and metadata from Global Data Assembly Centre (Argo GDAC). SEANOE. https://doi.org/10.17882/42182

AVISO: Altimeter satellite gridded sea level anomalies [Dataset], https://doi.org/10.48670/moi-00148, 2023.

Bell, J. D., Ganachaud, A., Gehrke, P. C., Griffiths, S. P., Hobday, A. J., Hoegh-Guldberg, O., Johnson, J. E., Le Borgne, R., Lehodey, P., Lough, J. M., Matear, R. J., Pickering, T. D., Pratchett, M. S., Senina, I., and Tribollet, A.: Mixed responses of tropical Pacific fisheries and aquaculture to climate change, Nat. Clim. Change, 3, 591–599, https://doi.org/10.1038/nclimate1838, 2013.

Bell, J. D., Kronen, M., Vunisea, A., Nash, W. J., Keeble, G., Demmke, A., Pontifex, S., and Andréfouët, S.: Planning the use of fish for food security in the Pacific, Mar. Policy, 33, 64–76, https://doi.org/10.1016/j.marpol.2008.04.002, 2009.

Bograd, S. J., Foley, D. G., Schwing, F. B., Wilson, C., Laurs, R. M., Polovina, J. J., Howell, E. A., and Brainard, R. E.: On the seasonal and interannual migrations of the transition zone chlorophyll front, Geophys. Res. Lett., 31, L17204, https://doi.org/10.1029/2004GL020637, 2004.

Bograd, S. J., Kang, S., Di Lorenzo, E., Horii, T., Katugin, O. N., King, J. R., Lobanov, V. B., Makino, M., Na, G., Ohman, M. D., Perry, R. I., Polovina, J. J., Putnam, H. M., Tadokoro, K., and Yoo, S.: Developing a social–ecological–environmental system framework to address climate change impacts in the North Pacific, Front. Mar. Sci., 6, 333, https://doi.org/10.3389/fmars.2019.00333, 2019.

Burd, A. B.: Modeling the vertical flux of organic carbon in the global ocean, Annu. Rev. Mar. Sci., 16, 135–161, https://doi.org/10.1146/annurev-marine-022123-102516, 2024.

Cai, W., Wang, G., Dewitte, B., Wu, L., Santoso, A., Takahashi, K., Yang, Y., Carréric, A., and McPhaden, M. J.: Increased variability of eastern Pacific El Niño under greenhouse warming, Nature, 564, 201–206, https://doi.org/10.1038/s41586-018-0776-9, 2018.

Calil, P. H., Richards, K. J., Jia, Y., and Bidigare, R. R.: Eddy activity in the lee of the Hawaiian Islands, Deep-Sea Res. Pt. II, 55, 1179–1194, https://doi.org/10.1016/j.dsr2.2008.01.008, 2008.

https://doi.org/10.5194/egusphere-2026-1877
Preprint. Discussion started: 29 July 2026

Carter, B. R., Bittig, H. C., Fassbender, A. J., Sharp, J. D., Takeshita, Y., Xu, Y.-Y., Álvarez, M., Wanninkhof, R., Feely, R. A., and Barbero, L.: New and updated global empirical seawater property estimation routines, Limnol. Oceanogr. Meth., 19, 785–809, https://doi.org/10.1002/lom3.10461, 2021.

Chelton, D. B., Schlax, M. G., and Samelson, R. M.: Summertime coupling between sea surface temperature and wind stress in the California Current System, J. Phys. Oceanogr., 37, 495–517, https://doi.org/10.1175/JPO3025.1, 2007.

Corno, G., Karl, D. M., Church, M. J., Letelier, R. M., Lukas, R., Bidigare, R. R., and Abbott, M. R.: Impact of climate forcing on ecosystem processes in the North Pacific Subtropical Gyre, J. Geophys. Res.-Oceans, 112, C04021, https://doi.org/10.1029/2006JC003730, 2007.

Couch, C. S., Huntington, B., Charendoff, J. A., Amir, C., Asbury, M., Basden, I., Lamirand, M., Torres-Pulliza, D., Brown, V., and Shantz, A. A.: Coral reef community recovery trajectories vary by depth following a moderate heat stress event at Swains Island, American Samoa, Mar. Biol., 171, 218, https://doi.org/10.1007/s00227-024-04533-z, 2024.

de Boyer Montégut, C.: Mixed layer depth over the global ocean: a climatology computed with a density threshold criterion of 0.03 kg/m3 from the value at the reference depth of 5 m, SEANOE, https://doi.org/10.17882/98226, 2024.

de Boyer, T. P., Garcia, H. E., Locarnini, R. A., Zweng, M. M., Mishonov, A. V., Reagan, J. R., Weathers, K. A., Baranova, O. K., Seidov, D., and Smolyar, I. V.: World Ocean Atlas 2018, https://www.ncei.noaa.gov/archive/accession/NCEI-WOA18 (last access: 29 September 2020), 2019.

De Carlo, E. H., Hoover, D. J., Young, C. W., Hoover, R. S., and Mackenzie, F. T.: Impact of storm runoff from tropical watersheds on coastal water quality and productivity, Appl. Geochem., 22, 1777–1797, https://doi.org/10.1016/j.apgeochem.2007.03.034, 2007.

De Falco, C., Desbiolles, F., Bracco, A., and Pasquero, C.: Island mass effect: a review of oceanic physical processes, Front. Mar. Sci., 9, 894860, https://doi.org/10.3389/fmars.2022.894860, 2022.

Doney, S. C., Ruckelshaus, M., Duffy, J. E., Barry, J. P., Chan, F., English, C. A., Galindo, H. M., Grebmeier, J. M., Hollowed, A. B., Knowlton, N., Polovina, J., Rabalais, N. N., Sydeman, W. J., and Talley, L. D.: Climate change impacts on marine ecosystems, Annu. Rev. Mar. Sci., 4, 11–37, https://doi.org/10.1146/annurev-marine-041911-111611, 2012.

Dore, J.E., R. Lukas, D.W. Sadler, M.J. Church, and D.M. Karl. Physical and biogeochemical modulation of ocean acidification in the central North Pacific. Proc Natl Acad Sci USA 106:12235-12240, 2009.

Doty, M. S. and Oguri, M.: The island mass effect, ICES J. Mar. Sci., 22, 33–37, https://doi.org/10.1093/icesjms/22.1.33, 1956.

Drenkard, E. J., Stock, C. A., Ross, A. C., Teng, Y. C., Cordero, T., Cheng, W., Curchitser, E., Dussin, R., Griffies, S. M., Hallberg, R., Harrison, M. J., Hedstrom, K., Jacox, M. G., Lehodey, P., Pozo Buil, M., Senina, I., and Zadeh, N.: A regional physical–biogeochemical ocean model for marine resource applications in the Northeast Pacific (MOM6-COBALT-NEP10k v1.0), Geosci. Model Dev., 18, 5245–5290, https://doi.org/10.5194/gmd-18-5245-2025, 2025.

https://doi.org/10.5194/egusphere-2026-1877
Preprint. Discussion started: 29 July 2026

Drenkard, E. J., Stock, C., Ross, A. C., Dixon, K. W., Adcroft, A., Alexander, M., Balaji, V., Bograd, S. J., Butenschön, M., Cheng, W., Curchitser, E., Edwards, C., Fiechter, J., Griffies, S., Haidvogel, D., Haynie, A. C., Hermann, A. J., Hofmann, E., Jacox, M., Siedlecki, S., and Wang, M.: Next-generation regional ocean projections for living marine resource management in a changing climate, ICES J. Mar. Sci., 78, 1969–1987, https://doi.org/10.1093/icesjms/fsab100, 2021.

Ducet, N., Le Traon, P. Y., and Reverdin, G.: Global high-resolution mapping of ocean circulation from TOPEX/Poseidon and ERS-1 and -2, J. Geophys. Res.-Oceans, 105, 19477–19498, https://doi.org/10.1029/2000JC900063, 2000.

Dueri, S., Bopp, L., and Maury, O.: Projecting the impacts of climate change on skipjack tuna abundance and spatial distribution, Global Change Biol., 20, 742–753, https://doi.org/10.1111/gcb.12460, 2014.

Dunne, J. P., Horowitz, L. W., Adcroft, A. J., Ginoux, P., Held, I. M., John, J. G., Krasting, J. P., Malyshev, S., Naik, V., Paulot, F., Shevliakova, E., Stock, C. A., Zadeh, N., Balaji, V., Blanton, C., Dunne, K. A., Dupuis, C., Durachta, J., Dussin, R., Gauthier, P. P. G., Griffies, S. M., Guo, H., Hallberg, R. W., Harrison, M., He, J., Hurlin, W., McHugh, C., Menzel, R., Milly, P. C. D., Nikonov, S., Paynter, D. J., Ploshay, J., Radhakrishnan, A., Rand, K., Reichl, B. G., Robinson, T., Schwarzkopf, D. M., Sentman, L. T., Underwood, S., Vahlenkamp, H., Winton, M., Wittenberg, A. T., Wyman, B., Zeng, Y., and Zhao, M.: The GFDL Earth System Model version 4.1 (GFDL-ESM 4.1): overall coupled model description and simulation characteristics, J. Adv. Model. Earth Sy., 12, e2019MS002015, https://doi.org/10.1029/2019MS002015, 2020.

Duteil, O., Oschlies, A., and Böning, C. W.: Pacific Decadal Oscillation and recent oxygen decline in the eastern tropical Pacific Ocean, Biogeosciences, 15, 7111–7126, https://doi.org/10.5194/bg-15-7111-2018, 2018.

Egbert, G. D. and Erofeeva, S. Y.: Efficient inverse modeling of barotropic ocean tides, J. Atmos. Ocean. Tec., 19, 183–204, https://doi.org/10.1175/1520-0426(2002)019<0183:EIMOBO>2.0.CO;2, 2002.

Flather, R.: A tidal model of the north-west European continental shelf, Mem. Soc. R. Sci. Liege, 10, 141–164, 1976.

Fox, H. E., Haisfield, K. M., Brown, M. S., Stevenson, T. C., Tissot, B. N., Walsh, W. J., and Williams, I. D.: Influences of oceanographic and meteorological features on reef fish recruitment in Hawai‘i, Mar. Ecol. Prog. Ser., 463, 259–272, https://doi.org/10.3354/meps09838, 2012.

Friedlander, A. M., Gove, J. M., Ballesteros, E., Esala, E., Fourriols, D., Makbrussman, J., Williams, I. D., and other authors: The state of coral reef ecosystems of the main Hawaiian Islands, NOAA Technical Memorandum NMFS-PIFSC, 56, 2018.

Friedrich, T., Powell, B. S., Stock, C. A., Hahn-Woernle, L., Dussin, R., and Curchitser, E. N.: Drivers of phytoplankton blooms in Hawaii: a regional model study, J. Geophys. Res.-Oceans, 126, e2020JC017069, https://doi.org/10.1029/2020JC017069, 2021.

Friedrich, T., Powell, B. S., Gunnarson, J. L., Liu, G., Giardina, S. F., Stuecker, M. F., Hošeková, L., Feloy, K., and Stock, C. A.: Submesoscale-permitting physical/biogeochemical future projections for the main Hawaiian Islands, J. Adv. Model. Earth Sy., 16, e2023MS003855, https://doi.org/10.1029/2023MS003855, 2024.

Galbraith, E. D. and Martiny, A. C.: A simple nutrient dependence mechanism for predicting the stoichiometry of marine ecosystems, P. Natl. Acad. Sci. USA, 112, 8199–8204, https://doi.org/10.1073/pnas.1423917112, 2015.

https://doi.org/10.5194/egusphere-2026-1877
Preprint. Discussion started: 29 July 2026

García, H. E., Weathers, K., Paver, C. R., Smolyar, I., Boyer, T. P., Locarnini, R. A., Zweng, M. M., Mishonov, A. V., Baranova, O. K., Seidov, D., and Reagan, J. R.: World Ocean Atlas 2018, Volume 3: dissolved oxygen, apparent oxygen utilization, and oxygen saturation, NOAA Atlas NESDIS 83, 38 pp., 2019a.

García, H. E., Weathers, K., Paver, C. R., Smolyar, I., Boyer, T. P., Locarnini, R. A., Zweng, M. M., Mishonov, A. V., Baranova, O. K., Seidov, D., and Reagan, J. R.: World Ocean Atlas 2018, Volume 4: dissolved inorganic nutrients (phosphate, nitrate and nitrate+nitrite, silicate), NOAA Atlas NESDIS 84, 35 pp., 2019b.

Garcia, H. E., Bouchard, C., Cross, S. L., Paver, C. R., Wang, Z., Reagan, J. R., Boyer, T. P., Locarnini, R. A., Mishonov, A. V., Baranova, O., Seidov, D., and Dukhovskoy, D.: World Ocean Atlas 2023, Volume 4: dissolved inorganic nutrients (phosphate, nitrate, silicate), NOAA Atlas NESDIS 92 [dataset], https://doi.org/10.25923/39qw7j08, 2023a.

Garcia, H. E., Wang, Z., Bouchard, C., Cross, S. L., Paver, C. R., Reagan, J. R., Boyer, T. P., Locarnini, R. A., Mishonov, A. V., Baranova, O., Seidov, D., and Dukhovskoy, D.: World Ocean Atlas 2023, Volume 3: dissolved oxygen, apparent oxygen utilization, and oxygen saturation, NOAA Atlas NESDIS 91 [dataset], https://doi.org/10.25923/rb67-ns53, 2023b.

Gove, J. M., McManus, M. A., Neuheimer, A. B., Polovina, J. J., Drazen, J. C., Smith, C. R., Merrifield, M. A., Friedlander, A. M., Ehses, J. S., Young, C. W., Dillon, A. K., and Williams, G. J.: Near-island biological hotspots in barren ocean basins, Nat. Commun., 7, 10581, https://doi.org/10.1038/ncomms10581, 2016.

Haidvogel, D. B., Arango, H., Budgell, W. P., Cornuelle, B. D., Curchitser, E., Di Lorenzo, E., Fennel, K., Geyer, W. R., Hermann, A. J., Lanerolle, L., Levin, J., McWilliams, J. C., Miller, A. J., Moore, A. M., Powell, T. M., Shchepetkin, A. F., Sherwood, C. R., Signell, R. P., Warner, J. C., and Wilkin, J.: Ocean forecasting in terrain-following coordinates: formulation and skill assessment of the Regional Ocean Modeling System, J. Comput. Phys., 227, 3595–3624, https://doi.org/10.1016/j.jcp.2007.06.016, 2008.

Hallberg, R.: Stable split time stepping schemes for large-scale ocean modeling, J. Comput. Phys., 135, 54–65, https://doi.org/10.1006/jcph.1997.5734, 1997.

Hallberg, R.: Using a resolution function to regulate parameterizations of oceanic mesoscale eddy effects, Ocean Model., 72, 92–103, https://doi.org/10.1016/j.ocemod.2013.08.007, 2013.

Hallberg, R. and Adcroft, A.: Reconciling estimates of the free surface height in Lagrangian vertical coordinate ocean models with mode-split time stepping, Ocean Model., 29, 15–26, https://doi.org/10.1016/j.ocemod.2009.02.008, 2009.

Hanich, Q., Wabnitz, C. C. C., Ota, Y., Amos, M., Donato-Hunt, C., and Hunt, A.: Small-scale fisheries under climate change in the Pacific Islands region, Mar. Policy, 88, 279–284, https://doi.org/10.1016/j.marpol.2017.11.011, 2018.

Hasegawa, D., Lewis, M. R., and Gangopadhyay, A.: How islands cause phytoplankton to bloom in their wakes, Geophys. Res. Lett., 36, L20605, https://doi.org/10.1029/2009GL039743, 2009.

Hersbach, H., Bell, B., Berrisford, P., Hirahara, S., Horányi, A., Muñoz-Sabater, J., Nicolas, J., Peubey, C., Radu, R., Schepers, D., Simmons, A., Soci, C., Abdalla, S., Abellan, X., Balsamo, G., Bechtold, P., Biavati, G., Bidlot, J., Bonavita, M., De Chiara, G., Dahlgren, P., Dee, D., Diamantakis, M., Dragani, R., Flemming, J., Forbes, R., Fuentes, M., Geer, A., Haimberger, L., Healy, S., Hogan, R. J., Hólm, E., Janisková, M., Keeley, S., Laloyaux, P.,

https://doi.org/10.5194/egusphere-2026-1877
Preprint. Discussion started: 29 July 2026

Lopez, P., Lupu, C., Radnoti, G., de Rosnay, P., Rozum, I., Vamborg, F., Villaume, S., and Thépaut, J.-N.: The ERA5 global reanalysis, Q. J. Roy. Meteor. Soc., 146, 1999–2049, https://doi.org/10.1002/qj.3803, 2020.

Hersbach, H., Bell, B., Berrisford, P., Biavati, G., Horányi, A., Muñoz Sabater, J., Nicolas, J., Peubey, C., Radu, R., Rozum, I., Schepers, D., Simmons, A., Soci, C., Dee, D., and Thépaut, J.-N.: ERA5 hourly data on single levels from 1940 to present, Copernicus Climate Change Service (C3S) Climate Data Store (CDS) [dataset], https://doi.org/10.24381/cds.adbb2d47, 2023.

Howell, E. A., Hawn, D. R., and Polovina, J. J.: Spatiotemporal variability in bigeye tuna (Thunnus obesus) dive behavior in the central North Pacific Ocean, Prog. Oceanogr., 86, 81–93, https://doi.org/10.1016/j.pocean.2010.04.013, 2010.

Huang, B., Liu, C., Banzon, V., Freeman, E., Graham, G., Hankins, B., Smith, T., and Zhang, H.-M.: Improvements of the Daily Optimum Interpolation Sea Surface Temperature (DOISST) Version 2.1, J. Climate, 34, 2923–2939, https://doi.org/10.1175/JCLI-D-20-0166.1, 2021.

Karl, D. M., Letelier, R., Hebel, D., Tupas, L., Dore, J., Christian, J. A., and Winn, C.: Ecosystem changes in the North Pacific subtropical gyre attributed to the 1991–92 El Niño, Nature, 373, 230–234, https://doi.org/10.1038/373230a0, 1995.

Karl, D. M. and Lukas, R.: The Hawaii Ocean Time-series (HOT) program: background, rationale and field implementation, Deep-Sea Res. Pt. II, 43, 129–156, https://doi.org/10.1016/0967-0645(96)00005-7, 1996.

Karl, D., Letelier, R., Tupas, L., Dore, J., Christian, J., and Hebel, D.: The role of nitrogen fixation in biogeochemical cycling in the subtropical North Pacific Ocean, Nature, 388, 533–538, https://doi.org/10.1038/41474, 1997.

Karl, D. M., Björkman, K. M., Dore, J. E., Fujieki, L., Hebel, D. V., Houlihan, T., Letelier, R. M., and Tupas, L. M.: Ecological nitrogen-to-phosphorus stoichiometry at station ALOHA, Deep-Sea Res. Pt. II, 48, 1529–1566, https://doi.org/10.1016/S0967-0645(00)00152-1, 2001.

Karl, D. M. and Church, M. J.: Ecosystem structure and dynamics in the North Pacific Subtropical Gyre: new views of an old ocean, Ecosystems, 20, 433–457, https://doi.org/10.1007/s10021-017-0117-0, 2017.

Kobayashi, D. R., Polovina, J. J., Parker, D. M., Kamezaki, N., Cheng, I. J., Uchida, I., Dutton, P. H., and Balazs, G. H.: Pelagic habitat characterization of loggerhead sea turtles, Caretta caretta, in the North Pacific Ocean (1997–2006): insights from satellite tag tracking and remotely sensed data, J. Exp. Mar. Biol. Ecol., 356, 96–114, https://doi.org/10.1016/j.jembe.2007.12.019, 2008.

Krasting, J. P., John, J. G., Blanton, C., McHugh, C., Nikonov, S., Radhakrishnan, A., Rand, K., Zadeh, N. T., Balaji, V., Durachta, J., Dupuis, C., Menzel, R., Robinson, T., Underwood, S., Vahlenkamp, H., Dunne, K. A., Gauthier, P. P. G., Ginoux, P., Griffies, S. M., Hallberg, R., Harrison, M., Hurlin, W., Malyshev, S., Naik, V., Paulot, F., Paynter, D. J., Ploshay, J., Reichl, B. G., Schwarzkopf, D. M., Seman, C. J., Silvers, L., Wyman, B., Zeng, Y., Adcroft, A., Dunne, J. P., Dussin, R., Guo, H., He, J., Held, I. M., Horowitz, L. W., Lin, P., Milly, P. C. D., Shevliakova, E., Stock, C., Winton, M., Wittenberg, A. T., Xie, Y., and Zhao, M.: NOAA-GFDL GFDL-ESM4 model output prepared for CMIP6 CMIP historical, Earth System Grid Federation [dataset], https://doi.org/10.22033/ESGF/CMIP6.8597, 2018.

https://doi.org/10.5194/egusphere-2026-1877
Preprint. Discussion started: 29 July 2026

Large, W. G. and Yeager, S. G.: Diurnal to decadal global forcing for ocean and sea-ice models: the data sets and flux climatologies, Tech. Rep., National Center for Atmospheric Research, https://doi.org/10.5065/D6KK98Q6, 2004.

Lehodey, P., Senina, I., and Murtugudde, R.: A spatial ecosystem and populations dynamics model (SEAPODYM) – modeling of tuna and tuna-like populations, Prog. Oceanogr., 78, 304–318, https://doi.org/10.1016/j.pocean.2008.06.004, 2008.

Lellouche, J. M., Greiner, E., Bourdallé-Badie, R., Garric, G., Melet, A., Drévillon, M., Bricaud, C., Hamon, M., Le Galloudec, O., Regnier, C., Candela, T., Testut, C.-E., Gasparin, F., Ruggiero, G., Benkiran, M., Drillet, Y., and Le Galloudec, O.: The Copernicus Global 1/12° oceanic and sea ice GLORYS12 reanalysis, Front. Earth Sci., 9, 698876, https://doi.org/10.3389/feart.2021.698876, 2021.

Letelier, R. M., Karl, D. M., Abbott, M. R., and Bidigare, R. R.: Light driven seasonal patterns of chlorophyll and nitrate in the lower euphotic zone of the North Pacific Subtropical Gyre, Limnol. Oceanogr., 49, 508–519, https://doi.org/10.4319/lo.2004.49.2.0508, 2004.

Letelier, R. M., Björkman, K. M., Church, M. J., Hamilton, D. S., Mahowald, N. M., Scanza, R. A., Schneider, N., White, A. E., and Karl, D. M.: Climate-driven oscillation of phosphorus and iron limitation in the North Pacific Subtropical Gyre, P. Natl. Acad. Sci. USA, 116, 12720–12728, https://doi.org/10.1073/pnas.1900789116, 2019.

Liu, G., Matrosova, L., Penland, J. E., Xu, G., Eakin, C. M., Christensen, T. R. L., Strong, A. E., Skirving, W. J., Geiger, E. F., and Heron, S. F.: Reef-scale thermal stress monitoring of coral ecosystems: new 5-km global products from NOAA Coral Reef Watch, Remote Sens., 6, 11579–11606, https://doi.org/10.3390/rs61111579, 2014.

Liu, G., Skirving, W. J., Geiger, E. F., De La Cour, J. L., Marsh, B. L., Heron, S. F., Murby, A. L., Strong, A. E., and Eakin, C. M.: NOAA Coral Reef Watch's 5km satellite coral bleaching heat stress monitoring product suite version 3 and four-month outlook version 4, Reef Encounter, 32, 39–45, 2017.

Liu, G., Eakin, C. M., Chen, M., Kumar, A., De La Cour, J. L., Heron, S. F., Geiger, E. F., Skirving, W. J., Tirak, K. V., and Strong, A. E.: Predicting heat stress to inform reef management: NOAA Coral Reef Watch's 4-month coral bleaching outlook, Front. Mar. Sci., 5, 57, https://doi.org/10.3389/fmars.2018.00057, 2018.

Liu, X., Stock, C. A., Dunne, J. P., Lee, M., Shevliakova, E., Malyshev, S., and Milly, P. C. D.: Simulated global coastal ecosystem responses to a half-century increase in river nitrogen loads, Geophys. Res. Lett., 48, e2021GL094367, https://doi.org/10.1029/2021GL094367, 2021.

Liu, G., Powell, B. and Friedrich, T.: Climate downscaling for regional models with a neural network: A Hawaiian example. Progress in Oceanography, 215, p.103047, https://doi.org/10.1016/j.pocean.2023.103047, 2023.

Manizza, M., Le Quéré, C., Watson, A. J., and Buitenhuis, E. T.: Bio-optical feedbacks among phytoplankton, upper ocean physics and sea-ice in a global model, Geophys. Res. Lett., 32, L05603, https://doi.org/10.1029/2004GL020778, 2005.

Martiny, A. C., Talarmin, A., Mouginot, C., Lee, J. A., Huang, J. S., Gellene, A. G., and Burger, J. M.: Biogeochemical controls of surface ocean phosphate, Sci. Adv., 5, eaax0341, https://doi.org/10.1126/sciadv.aax0341, 2019.

Meinshausen, M. and Vogel, E.: input4MIPs.UoM.GHGConcentrations.CMIP.UoM-CMIP1-2-0, Earth System Grid Federation [dataset], https://doi.org/10.22033/ESGF/input4MIPs.1118, 2016.

https://doi.org/10.5194/egusphere-2026-1877
Preprint. Discussion started: 29 July 2026

Meinshausen, M., Vogel, E., Nauels, A., Lorbacher, K., Meinshausen, N., Etheridge, D. M., Fraser, P. J., Montzka, S. A., Rayner, P. J., Trudinger, C. M., Krummel, P. B., Beyerle, U., Canadell, J. G., Daniel, J. S., Enting, I. G., Law, R. M., Lunder, C. R., O'Doherty, S., Prinn, R. G., Reimann, S., Rubino, M., Velders, G. J. M., Vollmer, M. K., Wang, R. H. J., and Weiss, R.: Historical greenhouse gas concentrations for climate modelling (CMIP6), Geosci. Model Dev., 10, 2057–2116, https://doi.org/10.5194/gmd-10-2057-2017, 2017.

Meinshausen, M. and Nicholls, Z. R. J.: UoM-MESSAGEGLOBIOM-ssp245-1-2-1 GHG concentrations, Earth System Grid Federation [dataset], https://doi.org/10.22033/ESGF/input4MIPs.9866, 2018.

Meinshausen, M., Nicholls, Z. R. J., Lewis, J., Gidden, M. J., Vogel, E., Freund, M., Beyerle, U., Gessner, C., Nauels, A., Bauer, N., Canadell, J. G., Daniel, J. S., John, A., Krummel, P. B., Luderer, G., Meinshausen, N., Montzka, S. A., Rayner, P. J., Reimann, S., Smith, S. J., van den Berg, M., Velders, G. J. M., Vollmer, M. K., and Wang, R. H. J.: The shared socioeconomic pathway (SSP) greenhouse gas concentrations and their extensions to 2500, Geosci. Model Dev., 13, 3571–3605, https://doi.org/10.5194/gmd-13-3571-2020, 2020.

Modular Ocean Model: MOM6, GitHub [code], https://github.com/mom-ocean/MOM6, last access: 2 February 2026.

Moeller, H. V., Laufkötter, C., Sweeney, E. M., and Johnson, M. D.: Light-dependent grazing can drive formation and deepening of deep chlorophyll maxima, Nat. Commun., 10, 1978, https://doi.org/10.1038/s41467-019-09591-2, 2019.

Morel, A.: Optical modeling of the upper ocean in relation to its biogenous matter content (case I waters), J. Geophys. Res.-Oceans, 93, 10749–10768, https://doi.org/10.1029/JC093iC09p10749, 1988.

Morel, A. and Maritorena, S.: Bio-optical properties of oceanic waters: a reappraisal, J. Geophys. Res.-Oceans, 106, 7163–7180, https://doi.org/10.1029/2000JC000319, 2001.

Moreno, A. R. and Martiny, A. C.: Ecological stoichiometry of ocean plankton, Annu. Rev. Mar. Sci., 10, 43–69, https://doi.org/10.1146/annurev-marine-121916-063126, 2018.

Moutin, T., Karl, D. M., Duhamel, S., Rimmelin, P., Raimbault, P., Van Mooy, B. A. S., and Claustre, H.: Phosphate availability and the ultimate control of new nitrogen input by nitrogen fixation in the tropical Pacific Ocean, Biogeosciences, 5, 95–109, https://doi.org/10.5194/bg-5-95-2008, 2008.

Negrete García, G., Matthews, . Dax ., Stock, C., Powell, B., Rykaczewski, R., Tanaka, K., Barkley, H., Friedrich, T., Ross, A. C., Luo, J. Y., & Teng, Y.-C. Model source code for initial submission of "A new ocean model for management of central North Pacific Marine Resources" to GMD" (HIC6kv1). Zenodo. https://doi.org/10.5281/zenodo.19478039, 2026a

Negrete García, G., Matthews, . Dax ., Stock, C., Powell, B., Rykaczewski, R., Tanaka, K., Barkley, H., Friedrich, T., Luo, J. Y., Ross, A. C., & Teng, Y.-C. Model input for initial submission of "A new ocean model for management of central North Pacific Marine Resources" to GMD (Version 1) [Data set]. Zenodo. https://doi.org/10.5281/zenodo.19485393, 2026b

Negrete García, G., Matthews, . Dax ., Stock, C., Powell, B., Rykaczewski, R., Tanaka, K., Barkley, H., Friedrich, T., Luo, J. Y., Ross, A. C., & Teng, Y.-C. Model output and analysis codes for initial submission of "A new ocean model for management of central North Pacific Marine Resources" to GMD (Version 1) [Data set]. Zenodo. https://doi.org/10.5281/zenodo.19486919, 2026c

https://doi.org/10.5194/egusphere-2026-1877
Preprint. Discussion started: 29 July 2026

NOAA Coral Reef Watch: NOAA Coral Reef Watch Version 3.1 daily 5km satellite regional virtual station time series data for American Samoa, Jan. 01, 1985–Apr. 15, 2023, NOAA Coral Reef Watch, https://coralreefwatch.noaa.gov/product/vs/data.php (last access: 12 December 2025), 2019.

NOAA-GFDL: MOM6, Github [code], https://github.com/NOAA-GFDL/MOM6, last access: 2 February 2026a

NOAA-GFDL: CEFI-regional-MOM6, Github [code], https://github.com/NOAA-GFDL/CEFI-regional-MOM6, last access: 2 February 2026b

Orlanski, I.: A simple boundary condition for unbounded hyperbolic flows, J. Comput. Phys., 21, 251–269, https://doi.org/10.1016/0021-9991(76)90023-1, 1976.

Perelman, J. N., Tanaka, K. R., Smith, J. N., and other authors: Subsurface temperature estimates from a Regional Ocean Modelling System (ROMS) reanalysis provide accurate coral heat stress indices across the Main Hawaiian Islands, Sci. Rep., 14, 6620, https://doi.org/10.1038/s41598-024-56865-x, 2024.

Peterson, R. N., Burnett, W. C., Glenn, C. R., and Johnson, A. G.: Quantification of point-source groundwater discharges to the ocean from the shoreline of the Big Island, Hawaii, Limnol. Oceanogr., 54, 890–904, https://doi.org/10.4319/lo.2009.54.3.0890, 2009.

Polovina, J. J., Howell, E., Kobayashi, D. R., and Seki, M. P.: The transition zone chlorophyll front, a dynamic global feature defining migration and forage habitat for marine resources, Prog. Oceanogr., 49, 469–483, https://doi.org/10.1016/S0079-6611(01)00036-2, 2001.

Polovina, J. J., Howell, E. A., Kobayashi, D. R., and Seki, M. P.: The transition zone chlorophyll front updated: advances from a decade of research, Prog. Oceanogr., 150, 79–85, http://dx.doi.org/10.1016/j.pocean.2015.01.006, 2017.

Poupon, M., Resplandy, L., and Luo, J.: Unifying framework reveals importance of dissolved fluxes in ocean biological carbon pump, preprint, Research Square, https://doi.org/10.21203/rs.3.rs-6666218/v1, 2025.

Prince, E. D. and Goodyear, C. P.: Hypoxia-based habitat compression of tropical pelagic fishes, Fish. Oceanogr., 15, 451–464, https://doi.org/10.1111/j.1365-2419.2005.00393.x, 2006.

Qiu, B.: Kuroshio Extension variability and forcing of the Pacific decadal oscillations: responses and potential feedback, J. Phys. Oceanogr., 32, 2465–2482, https://doi.org/10.1175/1520-0485(2003)033<2465:KEVAFO>2.0.CO;2, 2019.

Reichl, B. G. and Hallberg, R.: A simplified energetics based planetary boundary layer (ePBL) approach for ocean climate simulations, Ocean Model., 132, 112–129, https://doi.org/10.1016/j.ocemod.2018.10.004, 2018.

Renault, L., Molemaker, M. J., McWilliams, J. C., Shchepetkin, A. F., Lemarié, F., Chelton, D., Illig, S., and Hall, A.: Modulation of wind work by oceanic current interaction with the atmosphere, J. Phys. Oceanogr., 46, 1685–1704, https://doi.org/10.1175/JPO-D-15-0232.1, 2016.

Renault, L., Masson, S., Arsouze, T., Madec, G., and McWilliams, J. C.: Recipes for how to force oceanic model dynamics, J. Adv. Model. Earth Sy., 12, e2019MS001715, https://doi.org/10.1029/2019MS001715, 2019.

https://doi.org/10.5194/egusphere-2026-1877
Preprint. Discussion started: 29 July 2026

Reynolds, R. W., Smith, T. M., Liu, C., Chelton, D. B., Casey, K. S., and Schlax, M. G.: Daily high-resolution-blended analyses for sea surface temperature, J. Climate, 20, 5473–5496, https://doi.org/10.1175/2007JCLI1824.1, 2007.

Ringuet, S. and Mackenzie, F. T.: Controls on nutrient and phytoplankton dynamics during normal flow and storm runoff conditions, southern Kaneohe Bay, Hawaii, Estuaries, 28, 327–337, https://doi.org/10.1007/BF02693916, 2005.

Roberts, M. J., Baker, A., Blockley, E. W., Calvert, D., Coward, A., Hewitt, H. T., Jackson, L. C., Kuhlbrodt, T., Mathiot, P., Roberts, C. D., Schiemann, R., Seddon, J., Vannière, B., and Vidale, P. L.: Resolving and parameterising the ocean mesoscale in Earth System Models, Curr. Clim. Change Rep., 6, 137–152, https://doi.org/10.1007/s40641-020-00164-w, 2020.

Roemmich, D., Johnson, G. C., Riser, S., Davis, R., Gilson, J., Owens, W. B., Garzoli, S. L., Schmid, C., and Ignaszewski, M.: The Argo Program: observing the global ocean with profiling floats, Oceanography, 22, 34–43, https://doi.org/10.5670/oceanog.2009.36, 2009.

Ross, A. C., Stock, C. A., Adcroft, A., Curchitser, E., Hallberg, R., Harrison, M. J., Hedstrom, K., Zadeh, N., Alexander, M., Chen, W., Drenkard, E. J., du Pontavice, H., Dussin, R., Gomez, F., Griffies, S. M., Guo, H., Jacox, M. G., Jia, Y., Kleiner, T., Luo, J. Y., Martínez-Moreno, J., Pozo Buil, M., Raffa, F., Saba, V., and Werner, F.: A high-resolution physical-biogeochemical model for marine resource applications in the northwest Atlantic (MOM6-COBALT-NWA12 v1.0), Geosci. Model Dev., 16, 6943–6985, https://doi.org/10.5194/gmd-16-6943-2023, 2023.

Ross, A. C., Stock, C. A., Koul, V., Delworth, T. L., Lu, F., Wittenberg, A., and Alexander, M. A.: Dynamically downscaled seasonal ocean forecasts for North American East Coast ecosystems, Ocean Sci., 20, 1631–1656, https://doi.org/10.5194/os-20-1631-2024, 2024.

Sathyendranath, S., Brewin, R. J., Brockmann, C., Brotas, V., Calton, B., Chuprin, A., Cipollini, P., Couto, A. B., Dingle, J., Doerffer, R., Donlon, C., Dowell, M., Farman, A., Grant, M., Groom, S., Horseman, A., Jackson, T., Krasemann, H., Lavender, S., Martinez-Vicente, V., Mazeran, C., Mélin, F., Moore, T. S., Müller, D., Regner, P., Roy, S., Steele, C. J., Steinmetz, F., Swinton, J., Taberner, M., Thompson, A., Valente, A., Zühlke, M., Brockmann, C., and Platt, T.: An ocean-colour time series for use in climate studies: the experience of the Ocean Colour Climate Change Initiative (OC-CCI), Sensors, 19, 4285, https://doi.org/10.3390/s19194285, 2019.

Sathyendranath, S., Jackson, T., Brockmann, C., Brotas, V., Calton, B., Chuprin, A., Clements, O., Cipollini, P., Danne, O., Dingle, J., Donlon, C., Grant, M., Groom, S., Krasemann, H., Lavender, S., Mazeran, C., Mélin, F., Müller, D., Steinmetz, F., Valente, A., Zühlke, M., Feldman, G., Franz, B., Frouin, R., Werdell, J., and Platt, T.: ESA Ocean Colour Climate Change Initiative (Ocean_Colour_cci): Version 6.0, 4km resolution data, NERC EDS Centre for Environmental Data Analysis [dataset], https://dx.doi.org/10.5285/5011d22aae5a4671b0cbc7d05c56c4f0, 2023.

Schaefer, K. M., Fuller, D. W., and Block, B. A.: Movements, behavior, and habitat utilization of yellowfin tuna (Thunnus albacares) in the northeastern Pacific Ocean, ascertained through archival tag data, Mar. Biol., 152, 503–525, https://doi.org/10.1007/s00227-007-0689-x, 2005.

Seki, M. P., Polovina, J. J., Brainard, R. E., Bidigare, R. R., Leonard, C. L., and Foley, D. G.: Biological enhancement at cyclonic eddies tracked with GOES thermal imagery in Hawaiian waters, Geophys. Res. Lett., 28, 1583–1586, https://doi.org/10.1029/2000GL012439, 2001.

https://doi.org/10.5194/egusphere-2026-1877
Preprint. Discussion started: 29 July 2026

Senina, I., Lehodey, P., Sibert, J., and Hampton, J.: Integrating tagging and fisheries data into a spatial population dynamics model to improve its predictive skills, Can. J. Fish. Aquat. Sci., 77, 576–593, https://doi.org/10.1139/cjfas-2018-0470, 2020.

Sharp, J. D., Fassbender, A. J., Carter, B. R., Johnson, G. C., Schultz, C., and Dunne, J. P.: GOBAI-O2: temporally and spatially resolved fields of ocean interior dissolved oxygen over nearly 2 decades, Earth Syst. Sci. Data, 15, 4481–4518, https://doi.org/10.5194/essd-15-4481-2023, 2023.

Signell, R. P. and Geyer, W. R.: Transient eddy formation around headlands, J. Geophys. Res.-Oceans, 96, 2561–2575, https://doi.org/10.1029/90JC02029, 1991.

Skirving, W., Marsh, B., De La Cour, J., Liu, G., Harris, A., Maturi, E., Geiger, E., Eakin, C. M., and Strong, A.: CoralTemp and the Coral Reef Watch coral bleaching heat stress product suite version 3.1, Remote Sens., 12, 3856, https://doi.org/10.3390/rs12233856, 2020.

Smith, J. and Barkley, H.: In situ temperature time series across U.S. Pacific coral reefs, https://doi.org/10.25923/56nb-hh17, 2025.

Steinberg, D. K. and Landry, M. R.: Zooplankton and the ocean carbon cycle, Annu. Rev. Mar. Sci., 9, 413–444, https://doi.org/10.1146/annurev-marine-010814-015924, 2017.

Stock, C. A., Powell, T. M., and Levin, S. A.: Bottom–up and top–down forcing in a simple size-structured plankton dynamics model, J. Mar. Syst., 74, 134–152, https://doi.org/10.1016/j.jmarsys.2007.12.004, 2008.

Stock, C. A., Alexander, M. A., Bond, N. A., Brander, K. M., Cheung, W. W., Curchitser, E. N., Delworth, T. L., Dunne, J. P., Griffies, S. M., Haltuch, M. A., Hare, J. A., Hollowed, A. B., Lehodey, P., Levin, S. A., Link, J. S., Rose, K. A., Rykaczewski, R. R., Sarmiento, J. L., Stouffer, R. J., Schwing, F. B., Vecchi, G. A., and Werner, F. E.: On the use of IPCC-class models to assess the impact of climate on Living Marine Resources, Prog. Oceanogr., 88, 1–27, https://doi.org/10.1016/j.pocean.2010.09.001, 2011.

Stock, C. A., Dunne, J. P., and John, J. G.: Global-scale carbon and energy flows through the marine planktonic food web: an analysis with a coupled physical–biological model, Prog. Oceanogr., 120, 1–28, https://doi.org/10.1016/j.pocean.2013.07.001, 2014.

Stock, C. A., Pegion, K., Vecchi, G. A., Alexander, M. A., Tommasi, D., Bond, N. A., Fratantoni, P. S., Gudgel, R. G., Kristiansen, T., O'Brien, T. D., Xue, Y., and Yang, X.: Seasonal sea surface temperature anomaly prediction for coastal ecosystems, Prog. Oceanogr., 137, 219–236, https://doi.org/10.1016/j.pocean.2015.06.007, 2015.

Stock, C. A., Dunne, J. P., Fan, S., Ginoux, P., John, J., Krasting, J. P., Laufkötter, C., Paulot, F., and Zadeh, N.: Ocean biogeochemistry in GFDL's Earth System Model 4.1 and its response to increasing atmospheric CO2, J. Adv. Model. Earth Sy., 12, e2019MS002043, https://doi.org/10.1029/2019MS002043, 2020.

Stock, C. A., Dunne, J. P., Luo, J. Y., Ross, A. C., Van Oostende, N., Zadeh, N., Adcroft, A., Bianchi, D., Bopp, L., Boss, E., Brix, H., Buesseler, K., Doney, S. C., Dussin, R., Griffies, S., Hallberg, R., Harrison, M., and Teng, Y. C.: Photoacclimation and photoadaptation sensitivity in a global ocean ecosystem model, J. Adv. Model. Earth Sy., 17, e2024MS004701, https://doi.org/10.1029/2024MS004701, 2025.

Stramma, L., Johnson, G. C., Sprintall, J., and Mohrholz, V.: Expanding oxygen-minimum zones in the tropical oceans, Science, 320, 655–658, https://doi.org/10.1126/science.1153847, 2008.

https://doi.org/10.5194/egusphere-2026-1877
Preprint. Discussion started: 29 July 2026

Stramma, L., Schmidtko, S., Levin, L. A., and Johnson, G. C.: Ocean oxygen minima expansions and their biological impacts, Deep-Sea Res. Pt. I, 57, 587–595, https://doi.org/10.1016/j.dsr.2010.01.005, 2010.

Stramma, L., Prince, E. D., Schmidtko, S., Luo, J., Hoolihan, J. P., Visbeck, M., Wallace, D. W. R., Brandt, P., and Körtzinger, A.: Expansion of oxygen minimum zones may reduce available habitat for tropical pelagic fishes, Nat. Clim. Change, 2, 33–37, https://doi.org/10.1038/nclimate1304, 2012.

Stramma, L., Schmidtko, S., Bograd, S. J., Ono, T., Ross, T., Sasano, D., and Whitney, F. A.: Trends and decadal oscillations of oxygen and nutrients at 50 to 300 m depth in the equatorial and North Pacific, Biogeosciences, 17, 813–831, https://doi.org/10.5194/bg-17-813-2020, 2020.

Tsujino, H., Urakawa, L. S., Griffies, S. M., Danabasoglu, G., Adcroft, A. J., Amaral, A. E., Arsouze, T., Bentsen, M., Bernardello, R., Böning, C. W., Bozec, A., Chassignet, E. P., Danilov, S., Dussin, R., Exarchou, E., Fogli, P. G., Fox-Kemper, B., Guo, C., Ilicak, M., Jung, T., Kim, W. M., Lapin, V., Li, Y., Lin, P., Lindsay, K., Liu, H., Long, M. C., Komuro, Y., Marsland, S. J., Masina, S., Nummelin, A., Rieck, J. K., Ruprich-Robert, Y., Scheinert, M., Sicardi, V., Sidorenko, D., Suzuki, T., Tatebe, H., Wang, Q., Yeager, S. G., and Yu, Z.: Impact of increased horizontal resolution of an ocean model on carbon circulation in the North Pacific Ocean, J. Adv. Model. Earth Sy., 16, e2023MS003720, https://doi.org/10.1029/2023MS003720, 2024.

Van Oostende, N., Dussin, R., Stock, C., Barton, A., Curchitser, E., Dunne, J., and Ward, B.: Simulating the ocean's chlorophyll dynamic range from coastal upwelling to oligotrophy, Prog. Oceanogr., 168, 232–247, https://doi.org/10.1016/j.pocean.2018.10.009, 2018.

Venegas, R. M., Oliver, T., Liu, G., Heron, S. F., Clark, S. J., Pomeroy, N., Young, C., Eakin, C. M., and Brainard, R. E.: The rarity of depth refugia from coral bleaching heat stress in the western and central Pacific Islands, Sci. Rep., 9, 19710, https://doi.org/10.1038/s41598-019-56232-1, 2019.

Watkins-Brandt, K. S., Letelier, R. M., Spitz, Y. H., Church, M. J., Böttjer, D., and White, A. E.: Addition of inorganic or organic phosphorus enhances nitrogen and carbon fixation in the oligotrophic North Pacific, Mar. Ecol. Prog. Ser., 432, 17–29, https://doi.org/10.3354/meps09147, 2011.

Whitney, J. L., Gove, J. M., McManus, M. A., Smith, K. A., Lecky, J., Neels, J., Walton, A., Harding, D., Petersen, K., and Kobayashi, D. R.: Surface slicks are pelagic nurseries for diverse ocean fauna, Sci. Rep., 11, 3197, https://doi.org/10.1038/s41598-021-81407-0, 2021.

Wilkin, J. L.: The summertime heat budget and circulation of southeast New England shelf waters, J. Phys. Oceanogr., 36, 1997–2011, https://doi.org/10.1175/JPO2968.1, 2006.

Williams, P., Terawasi, P., and Reid, C.: Overview of tuna fisheries in the western and central Pacific Ocean, including economic conditions – 2016, Scientific Committee 13th Regular Session WCPFC, WCPFC-SC13-2017/GN-WP-01, Rarotonga, Cook Islands, 2017.

Woodworth-Jefcoats, P. A., Polovina, J. J., and Drazen, J. C.: Synergy among oceanographic variability, fishery expansion, and longline catch composition in the central North Pacific Ocean, Fish. Bull., 116, 228–239, https://doi.org/10.7755/FB.116.3.2, 2018.

Xie, S. P., Liu, W. T., Liu, Q., and Hashizume, M.: Far-reaching effects of the Hawaiian Islands on the Pacific Ocean–atmosphere system, Science, 292, 2057–2060, 10.1126/science.1059781, 2001.

https://doi.org/10.5194/egusphere-2026-1877
Preprint. Discussion started: 29 July 2026

1423 Zhuang, J., Dussin, R., Huard, D., Bourgault, P., Banihirwe, A., Raynaud, S., Malevich, B., Schupfner, M.,
1424 Fernandes, F., Levang, S., Gauthier, C., Jüling, A., Almansi, M., Scott, R., Rondeau-Genesse, G., Rasp, S., Smith,
1425 T. J., Stachelek, J., Plough, M., Manchon, P., Bell, R., Caneill, R., and Li, X.: xESMF: v0.8.2, Zenodo [code],
1426 https://doi.org/10.5281/zenodo.8356796, 2023.